Numerical Modeling of Liquid Geothermal Systems

USGS-PP--1044-D

DE83 902181

By M. L. Sorey

GEOHYDROLOGY OF GEOTHERMAL SYSTEMS

GEOLOGICAL SURVEY PROFESSIONAL PAPER 1044-D

PURCHASE ORDER NO. USGS-PP-1044-D
RECEIVED 6-21-83

UNITED STATES GOVERNMENT PRINTING OFFICE, WASHINGTON: 1978

DISTRIBUTION OF THIS DOCUMENT IS UNLIMITED

DISCLAIMER

This report was prepared as an account of work sponsored by an agency of the United States Government. Neither the United States Government nor any agency Thereof, nor any of their employees, makes any warranty, express or implied, or assumes any legal liability or responsibility for the accuracy, completeness, or usefulness of any information, apparatus, product, or process disclosed, or represents that its use would not infringe privately owned rights. Reference herein to any specific commercial product, process, or service by trade name, trademark, manufacturer, or otherwise does not necessarily constitute or imply its endorsement, recommendation, or favoring by the United States Government or any agency thereof. The views and opinions of authors expressed herein do not necessarily state or reflect those of the United States Government or any agency thereof.

DISCLAIMER

Portions of this document may be illegible in electronic image products. Images are produced from the best available original document.

UNITED STATES DEPARTMENT OF THE INTERIOR

CECIL D. ANDRUS, *Secretary*

GEOLOGICAL SURVEY

H. William Menard, *Director*

Sorey, M. L.
Numerical modeling of liquid geothermal systems.
(Geohydrology of geothermal systems)
(Geological Survey Professional Paper 1044-D)
Bibliography: p. 23-25
1. Geothermal resources--Mathematical models. I. Title. II. Series. III. Series: United States. Geological Survey. Professional Paper 1044-D
GB1199.5S67 551.4'9 78-606183

For sale by the Superintendent of Documents, U.S. Government Printing Office
Washington, D.C. 20402

Stock Number 024-001-03112-4

CONTENTS

ILLUSTRATIONS

TABLES

NOMENCLATURE

Symbol	*Description*	*Dimensions*
$A_{n,m}$	Surface area connecting nodes n and m	L^2
C	Compressibility coefficient	t^2/L^2
c	Specific heat at constant volume of fluid	L^2/t^2T
c_p	Specific heat at constant pressure of fluid	L^2/t^2T
c_s	Specific heat of solid phase	L^2/t^2T
D	Length of fault plane conduit	L
$D_{n,m}$	Distance between nodes n and m	L
$d_{n,m}$	Distance between node m and interface with node n	L
$\bar{g}$	Gravitational acceleration vector	L/t^2
H	Coefficient of surface heat transfer	M/t^2TL
K_m	Thermal conductivity of solid-fluid matrix	ML/t^3T
$\bar{\bar{K}}_c$	Thermal conductivity tensor for solid-fluid matrix	ML/t^3T
$\bar{\bar{K}}_d$	Coefficient of thermal dispersion	ML/t^3T
$\bar{\bar{K}}_m$	Total thermal dispersion tensor	ML/t^3T
k	Intrinsic permeability	L^2
L	Depth from land surface to source reservoir in hot spring models	L
M_c	Dimensionless mass flow rate in cylindrical hot spring model	—
M_p	Dimensionless mass flow rate in fault plane hot spring model	—
Nu	Nusselt number (dimensionless heat transfer coefficient)	—
P	Fluid pressure	M/Lt^2
Q	Lateral conductive heat loss from spring conduit	ML^2/t^3
Ra	Rayleigh number (natural convection parameter)	—
Ra_c	Critical Rayleigh number for onset of convection	—
r_c	Radius of cylindrical hot spring conduit	L
T	Temperature	T
T_b	Temperature at base of hot spring models	T
T_s	Temperature at land surface in hot spring models	T
t	Time	t
$\bar{v}_d$	Fluid flux vector or Darcian velocity	L/t
W	Half-width of fault plane conduit	L
α	Vertical compressibility of porous medium	Lt^2/M
β	Thermal expansivity of fluid	T^{-1}
γ	Coefficient in second order equation of state	T^{-2}
Θ	Interpolation factor in implicit/-explicit numerical scheme	—
Θ_{sp}	Dimensionless temperature of hot spring at land surface	—
κ	Fluid compressibility	Lt^2/M
μ	Fluid dynamic viscosity	M/Lt
ρ	Fluid density	M/L^3
$\overline{\rho c}$	Heat capacity of solid-fluid matrix	M/Lt^2T
ρ_0	Fluid density at reference state	M/L^3
ρ_s	Density of solid phase	M/L^3
$\bar{\bar{\tau}}$	Stress deviator tensor	M/Lt^2
τ_n	Time constant or stability limit node n	t
ϕ	Porosity	—

CONVERSION OF UNITS

Metric units are used throughout this report. Thermal parameters are reported in more familiar "working" units rather than in the now-standard SI (Systeme Internationale) units. The following table lists metric and equivalent U.S. Customary units, and "working" units and SI units for the thermal parameters.

Multiply metric units	*By*	
	Length	
centimeters (cm)	0.3937	inches (in)
meters (m)	3.281	feet (ft)
kilometers (km)	.6214	miles (mi)
	Area	
square centimeters (cm^2)	0.155	square inches (in^2)
square meters (m^2)	10.76	square feet (ft^2)
	Volume	
cubic centimeters (cm^3)	0.061	cubic inches (in^3)
	Mass	
gram (g)	3.528×10^{-2}	ounces (oz)
kilogram (kg)	2.205	pounds (lb)

Temperature: degrees Celsius to degrees Fahrenheit
$°F = 9/5°C + 32$

THERMAL PARAMETERS

Multiply "working" units	*By*	*To obtain SI units*
	Thermal Conductivity	
calories per centimeter second · degree Celsius ($cal\ cm^{-1}\ s^{-1}\ °C^{-1}$)	0.4187	watts per meter degree Kelvin ($Wm^{-1}\ °K^{-1}$)
	Heat Transfer Coefficient	
calories per square centimeter second degree Celsius ($cal\ cm^{-2}\ ^{-1}\ °C^{-1}$)	41.87	watts per square meter degree Kelvin ($Wm^{-2}°K^{-1}$)
	Heat Discharge	
calories per second ($cal\ s^{-1}$)	4.187	watts (W)
	Energy	
calories (cal)	4.187	joules (J)
	Specific Heat	
calories per gram · degree Celsius	4.187×10^3	joules per kilogram · degree Kelvin

GEOHYDROLOGY OF GEOTHERMAL SYSTEMS

NUMERICAL MODELING OF LIQUID GEOTHERMAL SYSTEMS

By M. L. SOREY

ABSTRACT

A mathematical model describing the physical behavior of hot-water geothermal systems is presented. The model consists of a set of coupled partial differential equations for heat and mass transfer in porous media and an equation of state relating fluid density to temperature and pressure. The equations are solved numerically using an integrated finite difference method which can treat arbitrary nodal configurations in one, two, or three dimensions.

The model is used to analyze cellular convection in permeable rock layers heated from below. Results for cases with constant fluid and rock properties are in good agreement with numerical and experimental results from other authors. Considering variations in fluid viscosity and thermal expansivity with temperature results in substantial differences in the values of the critical Rayleigh number for the onset of convection and the rate of vertical heat transfer compared with constant-parameter cases. For example, for a temperature difference of 300°C across a horizontal layer, the critical Rayleigh number based on parameters evaluated at the cold-side temperature is 2, whereas the corresponding constant-parameter value is $4\pi^2$. Numerical simulations of more realistic models for cellular convection show that for laterally-bound reservoirs, conduction of heat across the side walls can lower the vertical heat transfer rate through the reservoir by 40 percent. For unbounded reservoirs, simulating heat conduction in impermeable layers above and below the convecting layer lowered the rate of vertical heat transfer by 50 percent.

Heat and mass transfer associated with hot-spring systems was analyzed for cylindrical (isolated conduit) and plane symmetric (fault-plane) models. Results of numerical simulations yield non-dimensional relationships between spring discharge and temperature drop in the spring due to lateral conductive heat loss from the spring conduit. For the same spring discharge, the fault-plane model yields considerably greater conductive heat loss and temperature drop at springs than the cylindrical conduit model. Steady-state temperature distributions in the rock surrounding the conduit show the effects of this lateral heat flow out to distances of one conduit depth. The influence of convective motions in this region was investigated as a function of rock permeability. Finally, the time required for thermal equilibrium following hot-spring development can be estimated as $L^2/2\alpha$, where L is the conduit depth and α is the thermal diffusivity of the saturated rock.

INTRODUCTION

Geothermal systems are receiving increasing attention as an alternative source of energy; consequently, there is growing interest in understanding their nature and behavior. One approach to this problem is to attempt to deduce the physical behavior of such systems using a mathematical model. Such a model consists of a set of equations that describe the processes occurring within the system and the solution to these equations subject to conditions that prevail at a particular site.

The model approach has two important applications: the geothermal system under natural conditions before being disturbed by man, and the geothermal system during exploitation. Natural geothermal systems have been investigated by a great many workers. The main thrust of such studies has been to understand how geothermal systems can form and persist under the various geological constraints that can exist within the earth's crust. Mathematical modeling of the natural conditions of heat and fluid flow in a geothermal area can be used to describe certain basic phenomenon such as fluid convection induced by density imbalances and the associated convective heat transfer. Modeling also affords an economical alternative to an extensive drilling program in that various system properties such as reservoir volume and permeability can be inferred by using models to simulate known conditions and make parametric analyses.

The mathematical model can also be applied to the problem of evaluating the behavior of a geothermal system during exploitation. The main purpose, of course, is to estimate the quantity of recoverable energy and the rate at which mass and energy may be extracted. As information from drill holes and initial production characteristics becomes available, the model can be refined and used to simulate optimal development procedures.

Mathematical modeling of fluid and energy transfer in geothermal systems is a logical extension of similar techniques which have been successfully applied to the analysis of fluid flow in porous and fractured media. In geothermal areas we may need to consider the effects of density gradients on flow, heat transfer by conductive, convective, and dispersive mechanisms, and the simultaneous transfer of two fluid phases. Be-

cause of the complex nature of the equations and boundary conditions, numerical solutions are usually required, although analytical results are available for simplified cases. The development of general numerical models capable of treating all the complexities noted above is an area of considerable current interest. The purpose of this study is the development of a numerical model for single-phase fluid and heat transfer in three-dimensional porous media and the application of the model to problems involving natural convection and hot spring discharge in liquid geothermal systems before development.

PREVIOUS INVESTIGATIONS

No rigorous definition of what constitutes a geothermal system is really possible. In a general sense, we are concerned with areas of above-normal temperature and heat flow in which circulation of warm to hot fluids may be a significant process. Two broad types of geothermal systems involving water, that is hydrothermal systems, are recognized: liquid-dominated and vapor-dominated. The general characteristics of vapor-dominated systems in which steam is the continuous, pressure-controlling phase are discussed by White, Muffler and Truesdell (1971), Elder (1966), and James (1968). Most of the world's known hydrothermal systems are liquid-dominated, with water as the controlling pressure phase. The following discussion pertains mainly to liquid-dominated systems.

Mathematical modeling of hydrothermal systems has for a long time centered on the problem of convective heat transfer in a homogeneous porous layer heated from below. Early work by Lapwood (1948) and others followed the pattern of previous analyses of Benard convection in a layer of viscous fluid. This work was directed primarily at developing criteria for the onset of convective currents in a horizontal and laterally infinite permeable layer when the vertical temperature gradient exceeds a certain critical value. Beck (1972) extended the analysis of dynamic stability to a layer with lateral boundaries, that is—a box, and he developed criteria for the preferred shape and number of convection cells which form.

Many studies have been made of the increased rate of vertical heat transfer through a freely convecting horizontal porous layer. Analytical results have been reported by Wooding (1957, 1963), Donaldson (1962, 1968, 1970), and others; numerical and experimental results are given by Holst and Aziz (1972a, b), Combarnous and Bories (1973), and Horne and O'Sullivan (1974). Some work has also been done on the problem of an inclined porous layer bounded by isothermal surfaces as summarized by Combarnous and Bories (1973). They show that since the temperature gradient and gravity are no longer collineal, the fluid is constantly moving regardless of the temperature gradient. For the most part, previous investigations of the natural convection problem have treated one-layer systems with uniform boundary conditions and constant parameters. In the section on "Studies of Natural Convection," results using the numerical code developed in this study are compared with those previous investigations, and several more realistic models for natural convection are analyzed.

Another physical model used to describe hydrothermal systems is the pipe system, in which fluid is assumed to be channeled through zones of higher permeability in the rocks. Einarsson (1942) and Bodvarsson (1961) discuss the nature of thermal areas in Iceland in terms of pipe systems involving circulation of water to depths of 2–3 km and discharge in hot spring areas. Elder (1966) analyzed hydrothermal areas in Iceland and New Zealand using zero dimensional (lumped parameter), one-dimensional (pipe system), and multidimensional (homogeneous porous media) models to quantify the general features of heat and mass transfer. White (1957, 1961) used pipe systems to explain the chemical composition of waters associated with hydrothermal areas. A useful convective model analyzed by Donaldson (1968, 1970) consists of a permeable channel or reservoir at the base connecting recharge and discharge columns at the sides. Geometrical and physical parameters of the model, including the heat available at depth, can be adjusted to simulate the gross features of several types of hot water systems. This model is analyzed numerically (in the section on "Studies of Natural Convection") to evaluate effects of conducting side walls on circulatory convection in the discharge channel. Additional studies of natural convection in homogeneous porous media and pipe models are reviewed by Witherspoon, Newman, Sorey, and Lippman (1975).

Developments of the appropriate mathematical equations for heat and mass transfer in single-fluid porous media where Darcy's law is valid have been made by Bear (1972), and Fernandez (1972), and Mercer (1973). Combarnous and Bories (1973) and Green (1963) considered the adequacy of using a single equation for energy transfer in the solid-fluid matrix; this equation requires assuming thermal equilibrium at points of contact between the two phases. They also analyzed the relative magnitude of dispersive and conductive heat fluxes as discussed in the section on "Numerical Model". Equations for two-phase flow in porous media are presented by Bear (1972), Mercer, Faust, and Pinder (1974), and Witherspoon, Newman,

Sorey, and Lippman (1975). The common approach is to assume Darcian expressions for the flow of each phase and to combine them into a single flow equation under the assumption of equal pressure in both phases. The corresponding energy equation accounts for the effects of phase change, and the two-phase model can be applied to steam-water geothermal systems. Numerical solution of the coupled partial differential equations for mass and energy transfer by integral (Galerkin), finite element techniques is discussed by Mercer (1973) and Faust and Mercer (1975). Finite difference schemes were utilized by Holst and Aziz (1972a, b) and Horne and O'Sullivan (1974). A particular difficulty in numerical solution of transport equations is the generation of numerical dispersion error which can produce instabilities and spreading or smearing of temperature fronts. Lantz (1971) discusses the sources of these errors and methods for minimizing their effects.

Applications of numerical models to geothermal reservoir simulation are rather limited to date. Mercer (1973) attempted to simulate the Wairakei, New Zealand, thermal system under both steady state and exploitation conditions. At this stage his results are limited by the possible inadequacy of a two-dimensional areal model to simulate conditions in this system and the initiation of two-phase flow in the reservoir following several years of fluid production. Solutions to hypothetical two-phase reservoir problems are discussed by Lasseter, Witherspoon, and Lippman (1975) and Faust and Mercer (1975). Numerical models for steam stimulation in petroleum reservoirs have utilized similar equations and solution procedures as those applied to the geothermal problem (Weinstein and others, 1974; Coats and others, 1973).

The equations and numerical scheme used in this study are described in the section on "Numerical model". An integrated finite difference method is used, and solutions to the heat and fluid flow equations are interlaced in time. The model is applied to the problem of circulatory convection in permeable layers to demonstrate its capabilities and to extend the analysis to more realistic geometries and boundary conditions. Applications of numerical modeling to the transfer processes associated with hot spring systems are also presented.

ACKNOWLEDGMENTS

An earlier version of this paper constituted a doctoral dissertation in the Department of Civil Engineering, University of California, Berkeley. The study was done under the general direction of Paul A. Witherspoon, Jr., and Ralph Greif of the University of California and Arthur H. Lachenbruch of the U.S. Geological Survey. I am also indebted to I. G. Donaldson of the Department of Scientific and Industrial Research, Lower Hutt, New Zealand, and to T. J. Lasseter, Marcello Lippman, and T. N. Narasimhan, colleagues at the University of California, for valuable discussions and suggestions. T. J. Lasseter also assisted in developing the numerical procedures used in this study.

NUMERICAL MODEL

Macroscopic description of mass and energy transport in porous media has been developed from the microscopic level using principles of statistical mechanics. Bear (1972) and Fernandez (1972) present detailed discussions of the assumptions involved and the resulting equations. In this study we utilize the results of these authors, making certain simplifications to yield a set of two partial differential equations for the flow of water and heat and an equation of state relating fluid density to temperature and pressure.

PARTIAL DIFFERENTIAL EQUATIONS

FLOW EQUATION

To describe mathematically the flow processes in porous media, we must consider various properties such as pressure and temperature as averages over volume elements which are large compared with dimensions of individual pores and solid particles, but small compared with the dimensions of the exterior boundaries of the medium. This introduces the assumption of what Bear (1972, p. 19) terms a representative elementary volume or REV and allows the actual porous medium to be treated as a continuum in which average values of dependent variables can be assigned to mathematical points. Thus we can write an equation for the conservation of mass as

$$-(\nabla\cdot\rho\bar{v}_d) = \frac{\partial\phi\rho}{\partial t} \tag{1}$$

where ρ = fluid density, ϕ = porosity, t = time, and $\bar{v}_d$= fluid flux vector. The actual fluid velocity, averaged over the appropriate REV, would be equal to v_d/ϕ. The momentum equation for flow in porous media is

$$\nabla P+\nabla\cdot\bar{\bar{\tau}}-\rho\bar{g} = 0 \tag{2}$$

where P = fluid pressure, $\bar{\bar{\tau}}$ = stress deviator tensor, and $\bar{g}$ = gravitational acceleration vector. Equation 2 is obtained from the momentum equation for a homo-

geneous fluid system (as given by Bird and others, 1960, p. 79) by neglecting inertial forces $\left(\rho\frac{DV}{Dt}\right)$ which are small compared with viscous forces ($\nabla \cdot \bar{\bar{\tau}}$) for laminar flow in porous media. For isotropic porous media, the empirical observations of Darcy (1856) and the similarity with Poiseuille-type flow in small-diameter tubes leads to the relation

$$\nabla \cdot \bar{\bar{\tau}} = \frac{\mu}{k}\bar{v}_d \tag{3}$$

where μ = fluid viscosity and k = intrinsic permeability. Combining equations 2 and 3 yields

$$\bar{v}_d = -\frac{k}{\mu}(\nabla P - \rho\bar{g}) \tag{4}$$

or Darcy's law for laminar flow in isotropic porous media. For anisotropic media, Bear (1972, p. 105) and Raats and Klute (1968, p. 540) developed a similar expression for $\bar{v}_d$ in terms of a permeability tensor $\bar{\bar{k}}$. In this development, k will be treated as a scalar which can vary spacially, because in the geothermal systems we wish to model, little is known regarding the tensorial properties of $\bar{\bar{k}}$, and it is likely that large-scale inhomogeneities related to fractures and channeling will dominate the convective system.

Combining the continuity and momentum equations yields the flow equation

$$\nabla\cdot\rho\left[\frac{k}{\mu}(\nabla P - \rho\bar{g})\right] = \frac{\partial\phi\rho}{\partial t}. \tag{5}$$

For slightly compressible fluids such as water, we wish to solve the flow equation in terms of pressure rather than of density. Hence, we expand the right-hand side of (5) as

$$\frac{\partial\phi\rho}{\partial t} = \rho\frac{\partial\phi}{\partial P}\frac{\partial P}{\partial t} + \phi\left[\left(\frac{\partial\rho}{\partial P}\right)_T\frac{\partial P}{\partial t} + \left(\frac{\partial\rho}{\partial T}p\right)\frac{\partial T}{\partial t}\right]$$
$$= \rho\alpha\frac{\partial P}{\partial t} + \phi\rho\kappa\frac{\partial P}{\partial t} - \phi\rho\beta\frac{\partial T}{\partial t} \tag{6}$$

where κ = fluid compressibility, β = fluid thermal expansivity, and α = vertical compressibility of the porous medium. Following Remson, Hornberger, and Molz (1971) we assume that the velocity of solid particles is negligible and deformation of the solid matrix is significant only in the vertical direction. For the problems considered in this study, the thermal expansivity term $\phi\rho\beta\ \partial T/\partial t$ can be shown to be small compared with the compressibility terms $(\rho\alpha + \phi\rho\kappa)\ \partial P/\partial t$ owing to the large difference in response times between the thermal and hydraulic systems, that is $\partial T/\partial t << \partial P/\partial t$. Thus, we will neglect the expansivity term in equation 6 and write the final form of our flow equation as

$$\nabla\cdot\left(+\rho\frac{k}{\mu}\nabla P - \rho^2\bar{g}\frac{k}{\mu}\right) = C\frac{\partial P}{\partial t} \tag{7}$$

where $C = \rho\ (\phi\kappa + \alpha)$ = compressibility coefficient.

EQUATION OF STATE

We wish to consider density as a function of temperature and pressure. Following Fernandez (1972, p. 54) we can write

$$\rho = \rho_0 e^{-\beta(T-T_0)e^{\kappa}\ (P-P_0)} \tag{8}$$

where ρ_0 = fluid density at some reference state $(T_0 P_0)$. Expanding the exponentials in series form and retaining terms of first order yields

$$\rho = \rho_0[1-\beta(T-T_0)+\kappa(P-P_0)]\cdot \tag{9}$$

For geothermal applications where $(T-T_0)$ may be large, a more accurate form for the temperature dependence was suggested by Wooding (1957, p. 274) as follows:

$$\rho = \rho_0[1-\beta(T-T_0)-\gamma(T-T_0)^2]\cdot \tag{10}$$

Evaluating (ρ_0, T_0) at 25°C and setting $\beta = 3.17 \times 10^{-4}$ °C^{-1} and $\gamma = 2.56 \times 10^{-6}$ °C^{-2}, yields $\rho-\rho_0)$ to an accuracy of 2 percent in the range of 25°C to 300°C. Between 4°C and 25°C a first order expression can be used.

In comparing the magnitude of the effects of temperature and pressure on the calculation of fluid density, it is seen that, for liquid geothermal systems, the pressure dependence can usually be neglected. For example, assuming $(P-P_0)$ = 100 kg/cm^2 (equivalent to about 1,000 meters of head), $\kappa = 4.5 \times 10^{-5}$ cm^2/kg gives $(\rho-\rho_0)\rho_0 = \kappa\ (P-P_0) = 0.0045$. However, for $(T-T_0)$ = 100°C and $\beta = 5 \times 10^{-4}$ °C^{-1}, $(\rho-\rho_0)/\rho_0 = \beta\ (T_0-T) = 0.05$, an order of magnitude greater. Thus, in the numerical results that follow, equation 10 was utilized to compute fluid density except as discussed in the section on "Box Models". It should be noted, however, that in solving the flow equation 7 a portion of the density change with time is always derived from the fluid compressibility term $\phi\rho\kappa\partial P/\partial t$. In effect, then, density changes with pressure contribute to transient pressure changes, but calculated values of density are not updated as pressures change, only as temperature changes.

ENERGY EQUATION

The energy equation in porous media can be written

following Mercer (1973, p. 7) as

$$[\phi\rho c + (1-\phi)\,\rho_s c_s]\,\frac{\partial T}{\partial t} = \nabla\cdot\bar{\bar{K}}_m\cdot\nabla T - \rho\bar{v}_d c\cdot\nabla T \quad (11)$$

where ρ_s = density of solid phase, c_s = specific heat of solid phase, K_m = total thermal dispersion tensor, and c = specific heat at constant volume of fluid phase. This relationship is obtained by combining the corresponding energy equations for the solid and fluid phases, as developed by Bird, Stewart, Lightfoot and others (1960, p. 314), with terms accounting for energy increases by viscous dissipation and compression neglected. To obtain (11) several assumptions are made. First, we assume that the fluid and solid are in thermal equilibrium at each point of contact so that a single temperature, T, can be assigned to the saturated medium in a REV. This assumption has been shown to be valid for most porous media problems (Combarnous and Bories, 1973; Holst, 1970; and Green, 1963). However, a single energy equation may not be adequate under certain circumstances, such as forced convection at high flow rates through porous material with relatively low thermal conductivity (Curry, 1970; Combarnous and Bories, 1973). One can also envision difficulties in treating ground-water flow through fractured rock as porous media flow necessitating the use of an effective REV which is not small compared with the overall size of the system.

The flux of heat represented by $\bar{\bar{K}}_m\cdot\nabla T$ is a composite of heat conduction through the solid-fluid matrix and the spreading effects of dispersion in the fluid phase. Bear (1972, p.650) gives the components of the total thermal dispersion tensor as

$$\bar{\bar{K}}_m = \bar{\bar{K}}_c + \phi\,\bar{\bar{K}}_d \quad (12)$$

where $\bar{\bar{K}}_c$ = thermal conductivity tensor for solid-fluid matrix and $\bar{\bar{K}}_d$ = coefficient of thermal dispersion. Bear states that heat transfer by dispersion is analogous to mass transfer by hydrodynamic dispersion and results from the distribution of local velocities caused by the presence of grains and molecular diffusion. Mercer (1973, p. 10) develops the functional form of the thermal dispersion tensor as

$$K_{d_{ij}} = \epsilon_{ijkl}\,\frac{v_k v_l}{v} \quad (13)$$

where ϵ_{ijkl} = dispersivity of the medium, a fourth rank tensor, and v_k, v_l = components of velocity in the k and l directions, and v = magnitude of the velocity. Green (1963) has shown analytically and experimentally that for relatively uniform porous media, heat transfer due to dispersion is small compared with conduction for values of velocity normally encountered in ground water systems. Unfortunately, it is difficult to apply these laboratory results to field situations where considerable variability in permeability may increase the dispersive effect. Indeed, it is possible that where dispersion is important in heterogeneous systems, the assumption of thermal equilibrium between phases may also break down and a more complicated mathematical description for heat transfer will be required. With this in mind, and considering the absence of information as to the magnitudes of the tensorial components of (12), it seems reasonable to treat $\bar{\bar{K}}_m$ as a scalar K_m, which could represent an enhanced conductivity to account for dispersion. For example, Henry and Hilleke (1972, p. 33) used a value of K_m which was five times the static thermal conductivity to match the temperature distribution in a coastal salt water-fresh water aquifer. Thus, the energy equation 11 becomes

$$\overline{\rho c}\,\frac{\partial T}{\partial t} = \nabla\cdot K_m\nabla T - \rho\bar{v}_d c\cdot\nabla T \quad (14)$$

where $\overline{\rho c} = [\phi\rho c + (1-\phi)\,\rho_s c_s]$ = heat capacity of solid-fluid matrix.

NUMERICAL SOLUTION

The flow equation 7 is linear only if we neglect the pressure dependence of ρ and μ; however, both ρ and μ must be treated as functions of temperature, and thus the pressure and velocity fields depend on temperature. The energy equation 14 is nonlinear because of ρ (T) and c (T), and the temperature field depends on the velocity field. Thus, we must solve a coupled nonlinear set of equations. Further, in the geothermal systems we wish to study, properties such as permeability and thermal conductivity will vary spacially and the boundary geometry may be complex. For these reasons numerical solutions are required, and a code which can treat multidimensional problems with variable geometries would be desirable. A computer program for slightly compressible heat and fluid flow was therefore developed.

GENERAL PROCEDURE

The basic procedures in the program were derived from the work of Edwards (1969) and Lasseter (1974). Before writing finite difference approximations, we integrate the equations over the volume of a finite element and apply the divergence theorem to reduce the flux terms to integrals over the area of the element. Thus, for an equation of the form

$$\alpha\,\frac{\partial\lambda}{\partial t} = \nabla\cdot\beta\nabla\lambda \quad (15)$$

integration yields,

$$\int_{vol} \alpha \frac{\partial \lambda}{\partial t} dv = \int_{area} \beta \nabla\lambda \cdot d\bar{A} \cdot \quad (16)$$

To solve this equation numerically, we discretize the continuum into a finite series of elements, each with a specified volume and a surface area between it and surrounding elements. We must then assume that the volume-integrated factors on the left-hand side are constant over each element, and the surface-integrated terms are reasonably constant over each of the connecting areas.

Consider an element "n" and two adjacent elements $m1$ and $m2$ as shown below

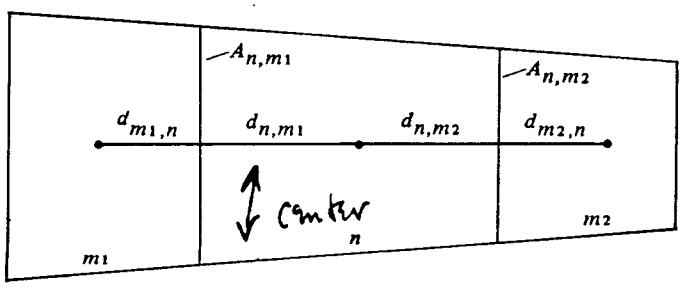

Writing equation 16 in difference form for this system yields

$$Vol_n \alpha_n \frac{\Delta\lambda n}{\Delta t} = A_{n,m1} \beta_{n,m1} (\nabla\lambda)_{n,m1} + A_{n,m2} \beta_{n,m2} (\nabla\lambda)_{n,m2} = \sum_m A_{n,m} \beta_{n,m} (\nabla\lambda)_{n,m} \cdot \quad (17)$$

To evaluate the flux at each interface, we assume that the average values of β and λ over the element apply at a particular point or node within the element. The gradient $(\nabla\lambda)_{n,m}$ is approximated as

$$(\nabla\lambda)_{n,m} = \frac{\lambda_m - \lambda_n}{d_{n,m} + d_{m,n}} \quad (18)$$

In general the distances $d_{n,m}$ and $d_{m,n}$ are measured normal to the interface $A_{n,m}$.

To preserve continuity of flux and potential across the interface, the coefficient $\beta_{n,m}$ must be evaluated as the harmonic mean of the values β_m for node m and β_n for node n. Thus

$$\beta_{n,m} = \frac{D_{n,m} \beta_n \beta_m}{\beta_n d_{m,n} + \beta_m d_{n,m}} \quad (19)$$

where $D_{n,m} = d_{n,m} + d_{m,n}$. Equation 17 can now be written

$$Vol_n \alpha_n \frac{\Delta\lambda n}{\Delta t} = \sum_m \frac{A_{n,m} \beta_n \beta_m}{\beta_n d_{m,n} + \beta_m d_{n,m}} (\lambda_m - \lambda_n). \quad (20)$$

The system of algebraic equations generated by writing equation 20 for each node in the system is solved by iteration. This general procedure puts no inherent restrictions on the number of nodes connected to node "n" or on the shape of the connecting surfaces. Thus it can be applied, as noted previously, to multidimensional problems with simple or complex element geometries. Narasimhan (1975) refers to this scheme as the IFD (Integrated Finite Difference Method) and gives a detailed conceptual comparison of the IFD method with the finite element method.

NUMERICAL FORMULATION OF FLOW EQUATION

The flow equation is

$$\nabla \cdot \left(+\rho \frac{k}{\mu} \nabla P - \rho^2 \bar{g} \frac{k}{\mu} \right) = C \frac{\partial P}{\partial t} \cdot \quad (7)$$

After volume integration, the difference equation can be written

$$C_n Vol_n \frac{\Delta P_n}{\Delta t} = \sum_m \left[\left(\frac{-\rho k A}{\mu} \right)_{n,m} \frac{(P_m - P_n)}{D_{m,n}} + \left(\frac{\rho^2 k A \eta g}{\mu} \right)_{n,m} \right] \quad (21)$$

where $\eta_{n,m}$ is the direction cosine of the angle between the outward normal of "n" towards "m" and the gravitational acceleration vector $\bar{g}$. Evaluating $(k/\mu)_{n,m}$ as the harmonic mean

$$\left(\frac{k}{\mu} \right)_{n,m} = \frac{D_{n,m} \left(\frac{k}{\mu} \right)_n \left(\frac{k}{\mu} \right)_m}{\left(\frac{k}{\mu} \right)_n d_{m,n} + \left(\frac{k}{\mu} \right)_m d_{n,m}} \quad (22)$$

and weighting the density by

$$\rho_{n,m} = \frac{d_{m,n} \rho_n + d_{n,m} P_m}{D_{n,m}} \quad (23)$$

we can rewrite equation 21 as

$$C_n Vol_n \frac{\Delta P_n}{\Delta t} = \sum_m \Psi_{n,m} (P_m - P_n) + \omega_{n,m} \quad (24)$$

where $\Psi_{n,m}$ = transductance = $\left[-\rho_{n,m} \left(\frac{k}{\mu} \right)_{n,m} \frac{A_{n,m}}{D_{n,m}} \right]$ and $\omega_{n,m} = \left[\rho^2_{n,m} \left(\frac{k}{\mu} \right)_{n,m} A_{n,m} \eta_{n,m} g \right]$.

We wish to solve the flow equation implicitly. Thus, we expand equation 24 into implicit and explicit parts as

$$C_n\, Vol_n\, \frac{\Delta P_n}{\Delta t} = \sum_m \{ [\, \Psi_{n,m}(P_m - P_n) + \omega_{n,m}\,] + \theta [\, \Psi_{n,m}\,(\Delta P_m - \Delta P_n)]\} \tag{25}$$

where P is the pressure at the old time and ΔP is the change in P during the time step Δt. The interpolation factor θ can be set to 1 for a fully implicit or backward differencing scheme, ½ for a Crank-Nicholson implicit scheme, or 0 for a fully explicit scheme. In solving the flow equation, θ is set to 1. The explicit part of equation 25 is computed first and then the implicit part is solved by iteration.

NUMERICAL FORMULATION OF ENERGY EQUATION

The energy equation 14 is

$$\overline{\rho c}\, \frac{\partial T}{\partial t} = \nabla \cdot K_m \nabla T - \rho \bar{v}_d c \cdot \nabla T \cdot \tag{14}$$

Before integrating, we rewrite this equation in divergence form as

$$\overline{\rho c}\, \frac{\partial T}{\partial t} = \nabla \cdot K_m \nabla T - \nabla \cdot \rho \bar{v}_d c T + T\, \nabla \cdot \rho \bar{v}_d c \cdot \tag{26}$$

The corresponding difference equation is

$$\left(Vol\, \overline{\rho c}\right)_n \frac{\Delta T_n}{\Delta t} = \sum_m \left[\left(KA\right)_{n,m} \frac{(T_m - T_n)}{D_{n,m}} + (\rho v_d c A)_{n,m}\, (T_{n,m} - T_n) \right] \tag{27}$$

where velocity is defined as positive into node n and $K_{n,m}$ is the harmonic mean conductivity.

Expanding into implicit and explicit terms yields

$$(Vol\, \overline{\rho c})_n \frac{\Delta T_n}{\Delta t} = \sum_m \{ [(KA)_{n,m} \frac{(T_m - T_n)}{D_{n,m}} + (\rho v_d c A)_{n,m}\, (T_{n,m} - T_n)] + \theta [(KA)_{n,m} \frac{(\Delta T_m - \Delta T_n)}{D_{n,m}} + (\rho v_d c A)_{n,m} \Delta T_{n,m}]\} \cdot \tag{28}$$

Temperature-dependent material properties are evaluated at some intermediate time between t and $t + \Delta t$. The procedure by which this point is determined is discussed by Lasseter (1974, App. C). The value of θ used to solve the energy equation is adjusted between 0.57 and 1.0 in order to damp out small oscillations in the solution.

The temperature at the interface $T_{n,m}$ could be evaluated by a linear interpolation

$$T_{n,m} = \frac{d_{m,n} T_n + d_{n,m} T_m}{D_{n,m}} . \tag{29}$$

It can be shown, however, and anticipated physically, that the temperature variation in the presence of convection is not linear and that the interface temperature is weighted in favor of the upstream node temperature. Numerically, it is also found that instabilities develop unless we use this upstream weighting. Thus, we rewrite equation 29 in terms of the adjusted distances $d'_{n,m}$ and $d'_{m,n}$ as

$$T_{n,m} = \frac{d'_{m,n} T_n + d'_{n,m} T_m}{D_{n,m}} . \tag{30}$$

The energy equation now becomes

$$(Vol\, \overline{\rho c})_n \frac{\Delta T_n}{\Delta t} = \sum_m [\Omega^1_{n,m}\, T_m + (\Omega^2 - \rho v_d c A)_{n,m} T_n] + \theta [\Omega^1_{n,m} \Delta T_m + \Omega^2_{n,m} \Delta T_n] \tag{31}$$

in terms of transductances

$$\Omega^1_{n,m} = [\left(\frac{KA}{D_{n,m}}\right) + (\rho v_d c A)_{n,m} \frac{d_{n,m}}{D_{n,m}}]$$

and

$$\Omega^2_{n,m} = [- \left(\frac{KA}{D_{n,m}}\right) + (\rho v_d c A)_{n,m} \frac{d'_{m,n}}{D_{m,n}}].$$

The instability noted above may develop if $\Omega^1_{n,m}$ and $\Omega^2_{n,m}$ have the same sign. To avoid this, we weight the interface temperature in favor of the upstream node temperature as follows. If $(\rho v_d)_{n,m}$, the mass flow rate from node "m" to "n", is large and positive, the transductances may both be positive. In this case the weighting $d'_{m,n}/D_{m,n}$ on T_m is reduced until $\Omega^2_{n,m}$ is just negative. If $(\rho v_d)_{n,m}$ is large and negative, the transductances will both be negative and the weighting $d'_{n,m}/D_{n,m}$ on T_m is reduced until $\Omega^1_{n,m}$ is positive. This computation is done internally by the computer program so that stability is always assured. The accuracy of this weighting technique was verified by Lasseter (1974) by comparing numerical results with analytical solutions for forced convection through porous media.

ITERATIVE SOLUTION

For each time step, the flow equation 25 is solved in a fully implicit fashion with the interpolation factor θ set to 1. With the energy equation 31, θ is adjusted between 0.57 and 1.0 and an implicit-explicit optimatization method is used. In the latter, a stability limit or time constant τ_n is defined for each node as

$$\tau_n = \frac{(Vol\ \overline{\rho c})_n}{\sum_m \Omega^*_{n,m}} \tag{32}$$

where $\Omega^*_{n,m}$ signifies that we sum the conductive components of $\Omega_{n,m}$ over all connections and take the difference between inflow and outflow of the convective components. τ_n represents the largest stable time step that could be used to solve equation 31 explicitly for node n. Physically, it is the approximate time required for a node to react significantly to changes in temperature of nodes it is connected to. Thus, for each time step, Δt, the energy equation is solved explicitly for nodes with $\tau_n < \Delta t$ and implicitly for all other nodes.

The time step used to solve the energy equation is controlled mainly by an input parameter, TVARY, which is the desired maximum temperature change per time step. For accuracy in transient problems, TVARY is set to about 1 percent of the maximum temperature change expected in the system. For steady state solutions, TVARY can be increased to speed convergence. Control of the time step for the flow equation is discussed in the next section.

Within each time step, the set of equations 31 for each node is solved by using the iterative technique developed by Edwards (1969) and discussed by Lasseter (1974). Convergence is generally rapid, but the number of iterations necessary depends on the relative number and time constant of interconnected nodes, the relative transductances for these connections, and TVARY which is used in the convergence test. The program adjusts Δt to optimize on about 40 iterations per time step.

COUPLING OF FLOW AND ENERGY EQUATIONS

Simultaneous solution of the flow and energy equations can be accomplished numerically by interlacing the solutions in time. Starting with initial temperature and pressure distributions at time t_0, we assume that temperatures are reasonably constant over a short interval of time and solve for a new pressure distribution at time $t_0 + \Delta t_0/2$. We then use this pressure distribution to determine the new temperature distribution at $t_0 + \Delta t$. These temperatures are then used to compute pressures at $t_0 + 3\Delta t/2$, and so on. This technique is illustrated in figure 1.

The actual scheme used is simplified due to the large difference between time constants of the two equations. The flow equation has time constants which are typically on the order of seconds while the energy equation has time constants on the order of tens of days. Thus after each temperature time step, the flow field will rapidly converge to a quasi-steady state solution. This is not a true steady state because temperatures are varying slowly with time and pressures will slowly but continually change. But we can solve for the quasi-steady state pressure distribution once we have computed a new temperature distribution without worrying about finding P and v_d at $\Delta t/2$. The difficulty with this technique is that many flow cycles per energy cycle are required to properly solve for the new pressure distribution because of the difference in time constants. A cycle is a step forward in time, whether it is a flow calculation or an energy calculation. For each temperature cycle, about 10 flow cycles are needed to compute the quasi-steady state solution. The time step for each flow cycle is adjusted to utilize about 40 iterations per cycle.

It should be noted that the equations presented and the problems solved in this paper do not involve source terms. With a mass source, such as a recharge or discharge well, the flow field would not necessarily equilibrate within each thermal cycle and the interlacing scheme shown in figure 1 would have to be followed.

STUDIES OF NATURAL CONVECTION

It is useful to identify two types of convective heat transfer in porous media. Forced convection results

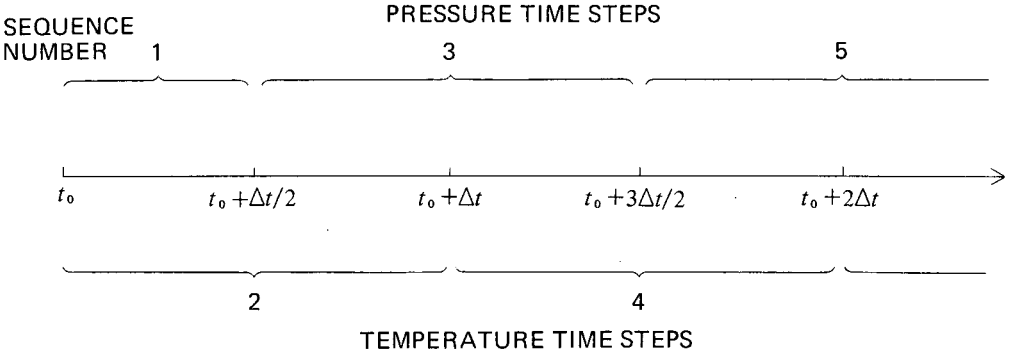

FIGURE 1.—Interlacing of temperature and pressure steps.

from externally imposed hydraulic conditions; fluid velocity is independent of the temperature distribution. Natural or free convection arises from buoyancy effects caused by temperature differences. In geothermal systems, both types of flow occur and convection could be termed mixed. One example of this mixed convection is the circulation of hydrothermal fluids from recharge areas to hot spring discharge areas. The driving force for this circulation, which may extend to depths of several kilometers, could be derived from a combination of the difference in elevation of the recharge and discharge areas and the density difference between the cold downflowing water and hot upflowing water.

CIRCULATORY CONVECTION

Of particular interest in geothermal studies is the phenomenon of circular or cellular convection. Consider a laterally extensive layer of permeable material heated from below as in figure 2. For the idealized condition where the upper and lower surfaces of the permeable layer are at constant temperatures T_0 and T_1, the conditions for the existence of the convective pattern shown are related to the dimensionless Rayleigh number, defined as in Witherspoon, Newman, Sorey, and Lippman, (1975) as

$$Ra = \frac{\beta g k (T_1 - T_0) L}{(K_m/\rho_0 c)(\mu/\rho_0)} \qquad (33)$$

where L = thickness of the permeable layer, and the other terms are as previously defined. The Rayleigh number relates buoyancy forces to viscous forces; and for the system in figure 2, Ra must exceed a critical value of $4\pi^2$ for convection to occur (Lapwood, 1948). For permeable layers with lateral boundaries, analytical results by Sutton (1969) and Beck (1972) can be used to determine the critical Rayleigh number (Ra_C) and the preferred convective mode as discussed below. The preferred convective mode refers to the number and shape of convective cells which would form at values of the Rayleigh number above Ra_C.

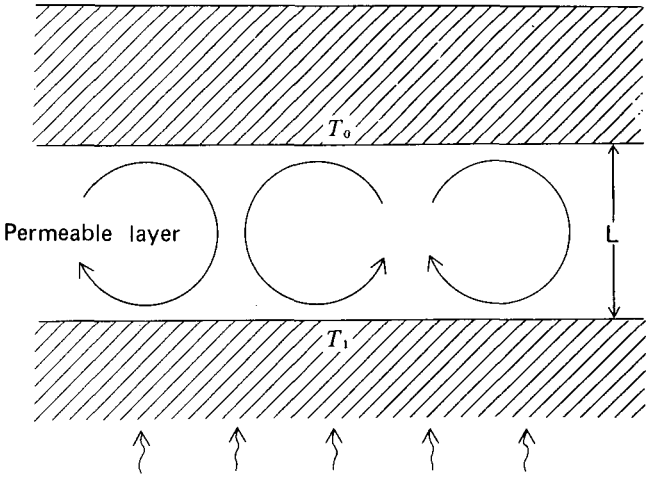

FIGURE 2.—Cellular convection in an extensive horizontal layer.

In real systems, it is doubtful that a critical Rayleigh number exists because there would be horizontal temperature variations along the upper and lower bounding surfaces. Convection is then set up for any value of $Ra>0$, provided the adiabatic temperature gradient $\partial T/\partial z = gT\beta/cp$ is exceeded (Landau and Lifshitz, 1959, p. 9). However, we would expect convective effects on the thermal and hydrologic regimes to be negligible except in geothermal areas with above normal heat flow and temperature gradients. Donaldson (1968) estimates that in geothermal areas the Rayleigh number is in the range of 500 to 5,000; and Horne and O'Sullivan (1974) estimate that in the Wairakei, New Zealand geothermal reservoir Ra is near 5,000.

Previous investigations of cellular convection in porous media have treated either the infinite layer case or box models with insulated, impermeable vertical sides. Results from box model studies have application to both laterally extensive aquifers where the zone of influence of each of the convection cells forms a box with respect to adjacent cells and to structurally bounded aquifers or channels. The effects of assumptions of isothermal surfaces above and below the aquifer and insulated side walls are discussed in the section on "Realistic Models." In the next section, a general description of heat and fluid flow in box model systems will be given and numerical results from the program developed for this study will be compared with analytical, experimental, and numerical results from other authors.

BOX MODELS

GENERAL CONSIDERATIONS

The geometry and boundary conditions for the box model are shown in figure 3. All sides are impermeable and the vertical sides are insulated. Following the analysis by Beck (1972), the problem of the onset of convection is solved by writing steady state forms of equations 7 and 14 for static conditions (no convection) and for a small disturbance upon the static state, under assumptions of constant coefficients and constant fluid density except in the gravity term of 7. The two sets of equations are subtracted and the resulting set of equations nondimensionalized. Solutions have been obtained by the linear and energy methods, both yielding the same result for the box model problem

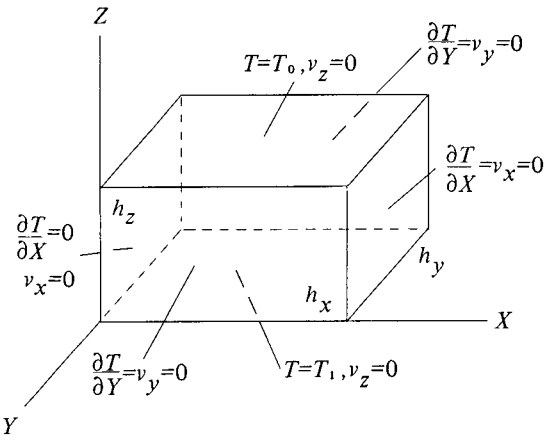

FIGURE 3.—Box model for cellular convection with heating from below.

(Beck, 1972). The critical Rayleigh number, which is the smallest eigenvalue of this eigenvalue problem, depends entirely on the aspect ratios h_x/h_z and h_y/h_z. The minimum value of Ra_c is $4\pi^2$ for the infinite layer case, and bounding the fluid tends to make it more stable, that is $Ra_c > 4\pi^2$.

For values of Ra just above the critical value, several modes of convection are possible. The motion can be either 2- or 3-dimensional with single or multiple cells. In contrast with the corresponding problem of free convection of an enclosed homogeneous fluid, 2-dimensional motion is possible because a no-slip boundary condition at the walls is not required for the porous media system. A roll is defined as a cell with only two non-zero velocity components. It has the appearance of a cylinder with axis parallel to the zero velocity coordinate. Beck's (1972) solution to the minimum eigenvalue problem shows that rolls are preferred over 3-dimensional cells whenever the height h_z is not the smallest dimension. When rolls do form, they are usually parallel to the shorter side, although the overriding rule is for the number of rolls and the direction of their axes to be such that each roll has the closest approximation to a square cross section as possible. For example, for $h_x = 2.0$, $h_y = 0.75$, and $h_z = 1.0$, two rolls form parallel to the y-axis as shown in figure 4. Three-dimensional cells occur when h_x, h_y, and h_z are nearly the same size, that is, a cube, and when the height h_z is less than both lateral dimensions. For a cube, the motion resembles a toroid with vertical axis through the center of the box. The velocity pattern in the (x,y) plane is shown in figure 5.

One effect of this convective motion is to increase the heat transferred vertically through the system. The Nusselt number Nu is defined as the ratio of heat flow with convection to heat flow by conduction in the absence of convection. For $Ra < Ra_c$, $Nu = 1$. In regard

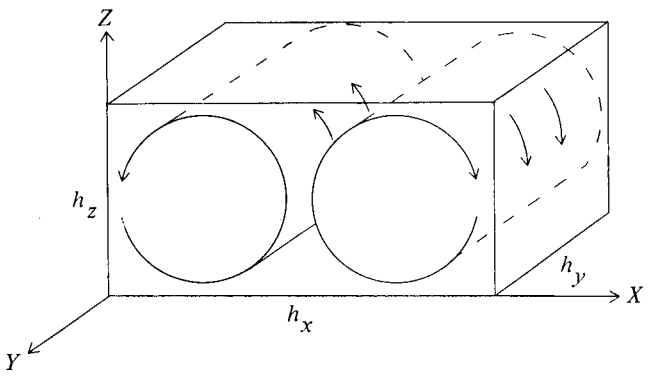

FIGURE 4.—Convective rolls in box with $h_x = 2\,h_z$.

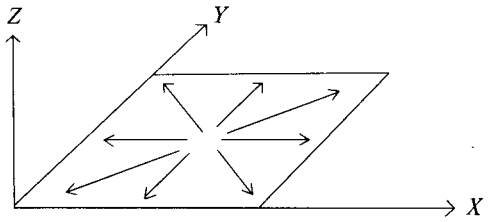

FIGURE 5.—Velocity pattern on lower surface of cube for three-dimensional convection.

to the number and shape of the convection cells which form at Rayleigh numbers above Ra_c, the analysis of Platzman (1965) indicates that the solution exhibiting the maximum heat transfer is physically preferred. Thus, for a square box with $Ra = 100$, a single roll for which $Nu = 2.60$ would be preferred over a two-roll mode for which $Nu = 2.20$. Numerical and experimental studies by Combarnous and Bories (1973) and Holst and Aziz (1972b) show that Nusselt numbers are not significantly different for two-and three-dimensional motions involving the same number of convection cells. Using the program code, comparison of plane symmetric, axisymmetric, and three-dimensional models with one convection cell at $Ra = 100$ yielded differences in Nu at steady state of less than 10 percent. In the discussions which follow, only two-dimensional convective motions are considered.

NUMERICAL SOLUTIONS

To model the box problem using the program, a 10×10 grid of nodes was normally used for 2-dimensional solutions and a $6 \times 6 \times 6$ grid for 3-dimensional solutions. The effect of grid spacing on the Nusselt number for a typical 2-dimensional problem is illustrated in figure 6 where the error for the 10×10 grid is only 3 percent of the extrapolated value for $\Delta x = \Delta y = 0$.

For most problems, only the steady state solution was desired. Hence, starting with initial temperature

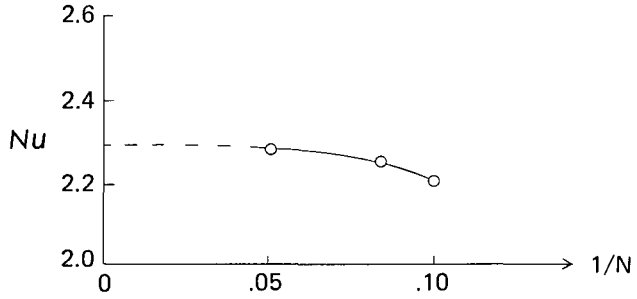

FIGURE 6.—Influence of grid spacing on steady state Nu, N = number of nodes in x and y directions.

and pressure conditions, the thermal time step was advanced rapidly using a large value of TVARY as discussed in the section on "Coupling of the Flow and Energy Equations"; steady state conditions were indicated when the hot and cold side Nusselt numbers became equal.

For a given aspect ratio, the choice of initial conditions affected the cellular pattern and the Nusselt number as steady state was approached. For example, using uniform initial temperature and pressure distributions in a square with Ra = 100 results in a 2-cell convective pattern with Nu = 2.20 as indicated in figure 7. If the initial temperature distribution is not symmetric, unicellular convection develops with Nu = 2.60 as shown in figure 8. In addition, Horne and O'Sullivan (1974) report that for a uniform initial temperature distribution in a square box, heating the lower boundary slowly instead of instantaneously, results in unicellular rather than multicellular motion. Thus, the convective pattern which may exist in a geothermal system probably depends, in part, on its thermal history.

The relationship between Ra and Nu determined numerically using the program is plotted in figure 9. These results are for a square, and the Nusselt number for each value of Ra corresponds to the cellular pattern which maximizes the heat transfer, which is the preferred cellular mode. As found numerically and experimentally by Combarnous and Bories (1973), the preferred cell size is a decreasing function of Rayleigh number, varying from an aspect ratio (width to height) of 1 at low values of Ra to an aspect ratio of 0.25 at Ra = 1,000. Also shown in figure 9 are numerical results from Combarnous and Bories (1973), obtained from finite difference solutions of nondimensional forms of equations 7 and 14. These authors also present experimental data for several combinations of porous materials and fluids. The Ra-Nu relationship in figure 9 fits with the average experimental results; variations between the different experimental systems were attributed to finite heat transfer coefficients at solid-fluid contacts. However,

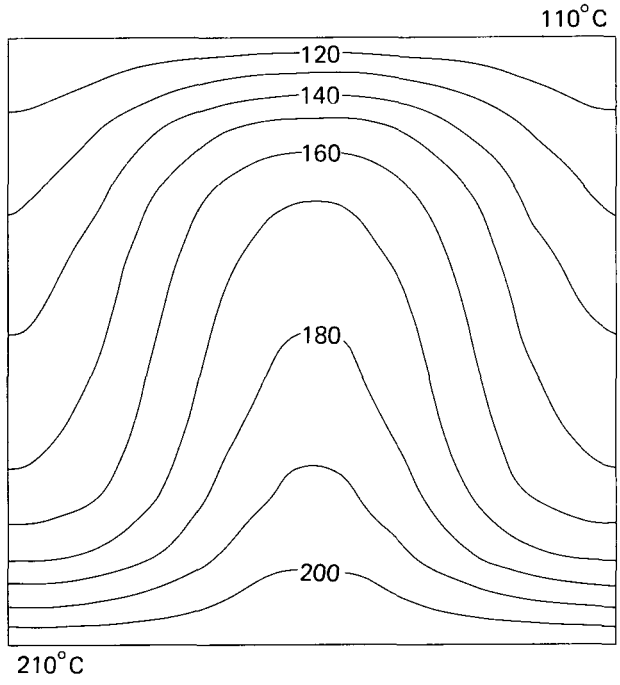

FIGURE 7.—Steady-state temperature distribution obtained from uniform (symmetric) initial temperature distribution.

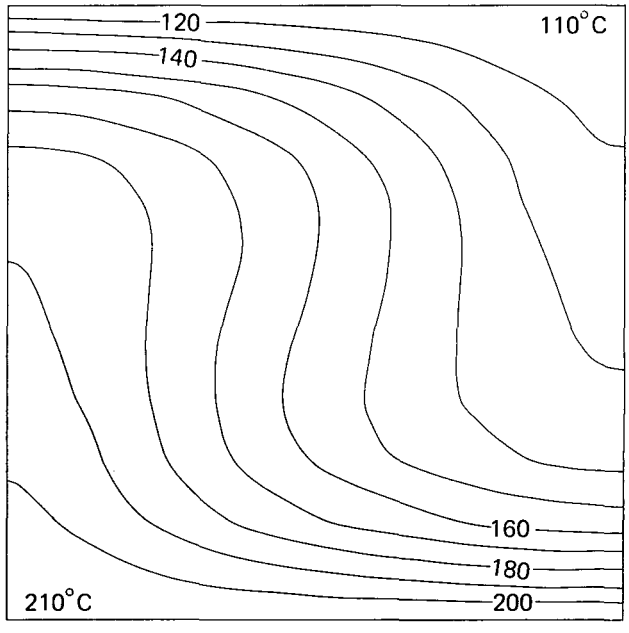

FIGURE 8.—Steady-state temperature distribution obtained from nonuniform (asymmetric) initial temperature distribution.

for materials with thermal conductivity K_m between 2 and 5 mcal/(s, °C cm) (for example, natural earth materials), the numerical model assuming an infinite heat transfer coefficient was found to be adequate.

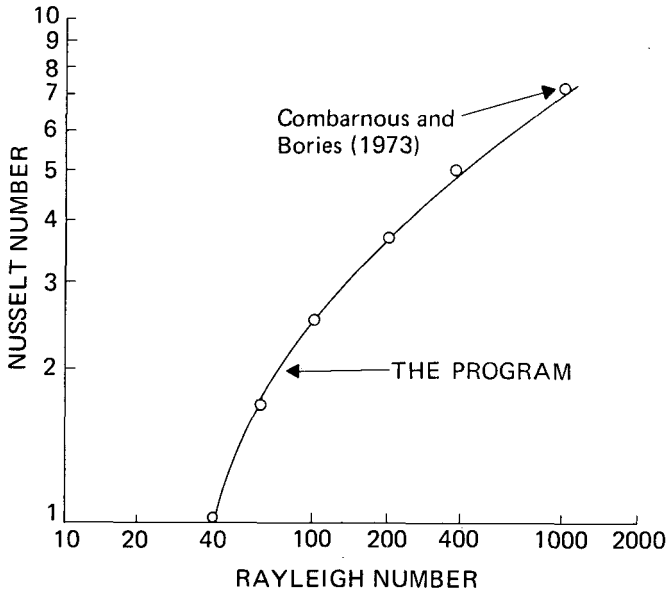

FIGURE 9.—The relationship between *Ra* and *Nu* determined numerically for cellular convection in box model.

The existence of oscillatory or fluctuating convective states has been investigated by Horne and O'Sullivan (1974) and Caltagirone, Cloupean, and Combarnous (1971) for box models in which the lower boundary is uniformly and nonuniformly heated. Their work includes experimental and numerical observations of regular and irregular variations in the convection cell pattern and the resultant Nusselt number at Rayleigh numbers above about 300. Real time periods for these fluctuations at *Ra* near 1,000 were approximately equal to the expression $(0.006\ L^2\overline{\rho c}/K_m)$, which yields a range from 200 to 700 years for typical thermal properties in systems with L near 1 Km². Corresponding variations in Nusselt number of ± 15 percent were found. Numerical simulations using the program for the uniformly heated case indicate similar instabilities at a Rayleigh number of 1,000 for motion which is dominantly unicellular, although the Nusselt number variation was only ±6 percent. Thus, from the standpoint of modeling natural convection in geothermal systems, the rather large periodicity and limited quantitative effect on heat flow associated with this oscillatory phenomenon suggest that its practical significance may be limited.

TEMPERATURE-DEPENDENT PARAMETERS

In previous studies of the critical Rayleigh number and the *Ra-Nu* relationship, the properties μ and c were treated as constants and the first-order equation of state (9) was used to relate fluid density to temperature. In the program the relationships $\mu\ (T)$ and $c\ (T)$ can be tabulated or suitable analytical expressions can be solved at each thermal time step. Table 1 lists values of ρ, c, and μ for pure water at temperatures covering the range found in hydrothermal systems. The viscosity variation with temperature is considerably larger than that for density or specific heat, and the variation suggests that results obtained with a constant viscosity assumption may be significantly in error. Actually, thermal expansivity β, which appears in the equation (33) for Rayleigh number, increases considerably with temperature and further complicates the analysis.

TABLE 1. *Temperature-dependent properties of pure water*

[From Dorsey (1968)]

T (°C)	P (atm)	ρ (g/cm³)	μ (g/m-s)	c (cal/°C g)
10	1	1.000	1.307	1.000
60	1	.983	.467	.951
160	50	.910	.174	.833
260	50	.788	.109	.763
310	100	.692	.090	.741

The combined effects of the temperature dependence of ρ, c, μ, and β on the analysis of cellular convection were evaluated for a box model with aspect ratio of 1.0. The *Nu-Ra* relationship was examined for several values of the vertical temperature difference $(T_1\text{-}T_0)$, using an average temperature in each case of 160°C. The second-order relation (eq. 10) for $\rho(T$ was used and permeability k was adjusted to keep *Ra* constant as $(T_1\text{-}T_0)$ varied. For each run, two Rayleigh numbers were calculated. One could be termed the cold-side Rayleigh number Ra_0, where

$$Ra_0 = \frac{gkL(T_1-T_0)}{K_m}\left[\frac{\rho_0^2 c_0 \beta_0}{\mu_0}\right] \tag{34}$$

and the subscript (0) indicates evaluation at $T = T_0$. A mean Rayleigh number Ra_m was also computed as

$$Ra_m = \frac{gkL(T_1-T_0)}{K_m}\left[\frac{\rho_0^2 c_m \beta_e}{\mu_m}\right] \tag{35}$$

where the subscript (m) indicates evaluation at $T = (T_1\text{-}T_0)/2 = 160°C$, and β_e is an effective expansivity computed as

$$\beta_e = \frac{\rho_0-\rho_1}{\rho_0(T_1-T_0)}. \tag{36}$$

For each (T_1-T_0), eight-point tabulations of $\mu(T)$ and $c(T)$ were used with linear interpolation between points.

The results are shown in figure 10. The heavy solid curve is the same as the curve in figure 9 for the constant parameter case. We note that for a given system, computing the Rayleigh number based on μ, c, and β

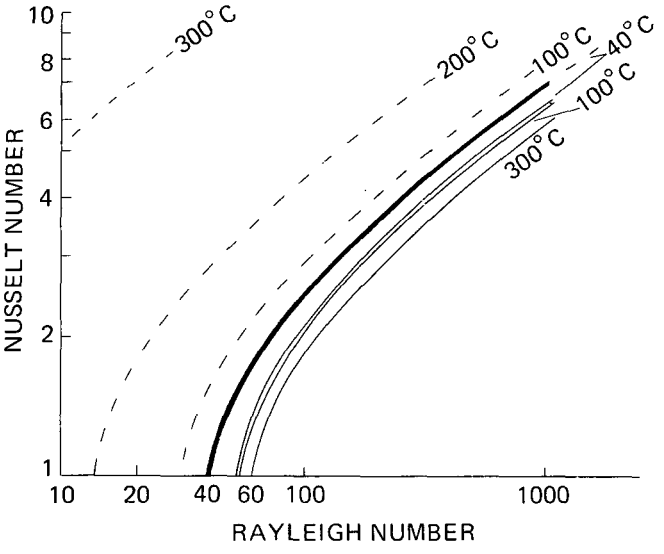

FIGURE 10. — Nusselt number with temperature-dependent fluid properties as a function of cold-side Rayleigh number (eq. 34, dashed lines) and mean Rayleigh number (eq. 35, solid lines) for temperature differences T_1-T_0 between 40°C and 300°C. Critical Rayleigh numbers at Nu = 1.0. Heavy solid line is for properties independent of T (see fig. 9).

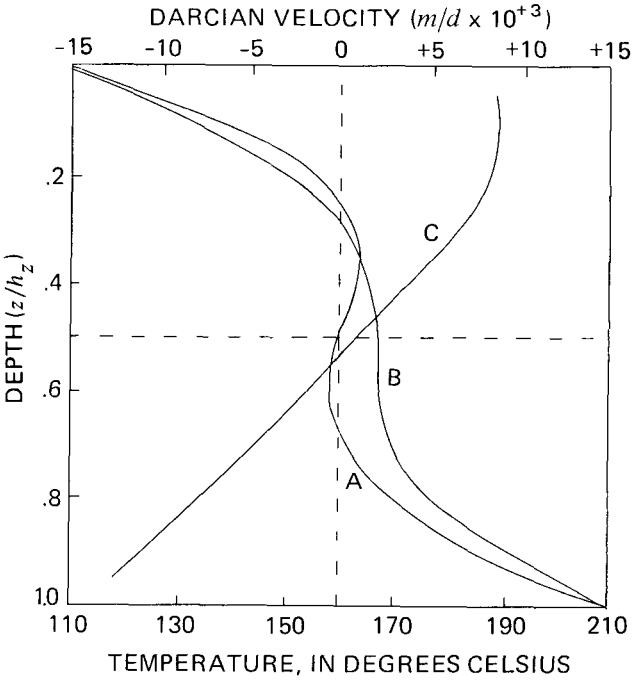

FIGURE 11.—Temperature and velocity profiles at midplane ($x = h_x/2$) for convection cell with Ra_m = 100 and T_1-T_0 = 100°C. Temperature curve A is for constant fluid properties; temperature curve B and velocity curve C are for temperature-dependent fluid properties.

evaluated at T_0 yields a value of Nu which increases with (T_1-T_0) and is greater than the constant parameter result for (T_1-T_0) greater than about 40°C. In contrast, the Nusselt number corresponding to Ra_m is less than the constant parameter result and decreases with (T_1-T_0). The position of the Nu-Ra_m curves may vary with the actual average temperature $(T_1-T_0)/2$ due to nonlinearities in the $\mu(T)$, $c(T)$, $\rho(T)$ relations, but the choice of $(T_1-T_0)/2$ = 160°C should be representative of geothermal reservoirs. The explanation for the lower heat transfer with variable fluid properties (Nu-Ra_m) may also be related to the nonlinearity in $\mu(T)$ which causes the centroid value of μ for $T_0 \leq T \leq T_1$ to be greater than μ at $(T_1-T_0)/2$. Because Ra is inversely proportional to μ, the effective Ra should be less than Ra_m. A similar trend of decreasing heat transfer with increasing (T_1-T_0) was reported by Holst and Aziz (1972a) with n-heptane as the convecting fluid.

Results in figure 10 also show that the critical Rayleigh number is influenced by variable fluid properties. In terms of the cold-side Rayleigh number Ra_0 the onset of convection occurs near the theoretical value of $4\pi^2$ for (T_1-T_0) < about 40°C but occurs at values of $Ra < 4\pi^2$ for (T_1-T_0) > 40°C. For (T_1-T_0) = 300°C, the critical value of Ra_0 is only 1.7. However, the critical value in terms of Ra_m is always greater than $4\pi^2$, reaching a value of 61 for a temperature difference of 300°C. Finally it should be noted that variable fluid properties also cause the temperature and flow patterns to be asymmetric as shown in figure 11. The asymmetry reflects the fact that the hotter, less viscous fluid near the bottom moves more easily than the colder fluid above.

EFFECT OF DENSITY VARIATION WITH PRESSURE

The effects of allowing fluid density to vary with pressure according to equation 7 were evaluated for the system shown in figure 12. Two runs were made, one with ρ (T) and one with $\rho = \rho$ (T,P), for (T_1-T_0) = 1°C and 100°C. For a temperature difference of 100°C across the box, the effect of temperature on density should dominate, as discussed in the section on "Partial Differential Equations." However, for a temperature difference of 1°C, the density increase from top to bottom due to the increase in hydrostatic pressure is 10 times the density decrease due to the temperature difference.

The results of the computer runs are listed in table 2. Although the Nusselt number for run 4 with $\rho = \rho$ (T,P) is slightly higher than the value for run 3 with $\rho = \rho$ (T), the difference in heat transfer between the various runs were negligible. Similarly, temperature and velocity distributions were essentially the same for each run. Thus, for problems or circulatory convection in porous media, density can probably be considered a function of temperature only.

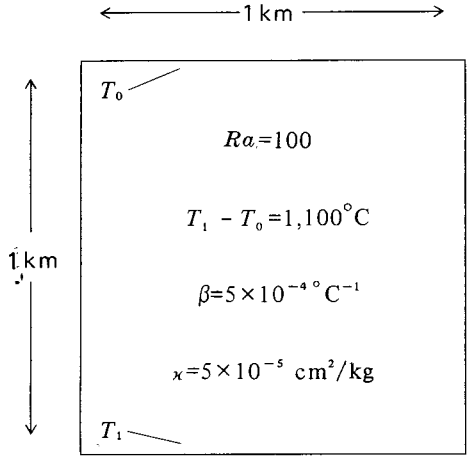

FIGURE 12.—Box model to test effects of density variation with pressure.

TABLE 2.—*Results of computer runs with density a function of pressure*

Run	T_1-T_0 (°C)	ρ	Nu
1 _____	100	ρ (T)	2.60
2 _____	100	ρ (T,P)	2.60
3 _____	1	ρ (T)	2.60
4 _____	1	ρ (T,P)	2.61

REALISTIC MODELS

Application of results from box model investigations are somewhat limited because the boundary conditions are not realistic. In particular, the assumptions of insulated sides and constant temperature at the top and bottom of the convecting layer may not hold in the field problem. It is possible, however, to use the numerical code to evaluate the effects of these assumptions on temperature distributions and heat transfer rates.

CONDUCTING SIDE WALLS

Consider the model shown in figure 13 which is similar to one proposed by Donaldson (1968, 1970) for simulation of convecting geothermal systems. The permeable channel, labeled B, could represent a fractured zone of upflowing liquid, separated from a recharge area with downflowing water by impermeable blocks, labeled A. A horizontal channel connecting the recharge and discharge areas is not shown at the bottom of this model because our interest here is on circulatory convection in the vertical channel. For this reason we also treat the upper and lower surfaces of Channel B as impermeable. A constant temperature T_0 is imposed along the top and sides, and a linear temperature variation from T_0 to T_1 is imposed along the bottom of the blocks A. The bottom of channel B is maintained at T_1, and the vertical sides of the channel are impermeable but thermally conductive.

For a particular case in which T_1-T_0 = 100°C, w/L = 2.1, and y/L = 0.5, and a Rayleigh number for the channel of 100, the temperature distribution shown in figure 14 would result. The temperature distribution for the case of conduction only (Ra = 0) is also shown and was used as a reference in computing the Nusselt number to account for the influence of the distance w and the temperature T_0 imposed at the sides of the model. Heat transfer rates along various boundaries are listed in table 3.

The Nusselt number for the channel is 1.3, compared with a value of 2.2 determined for the corresponding box model with insulated sides as in figure 7.

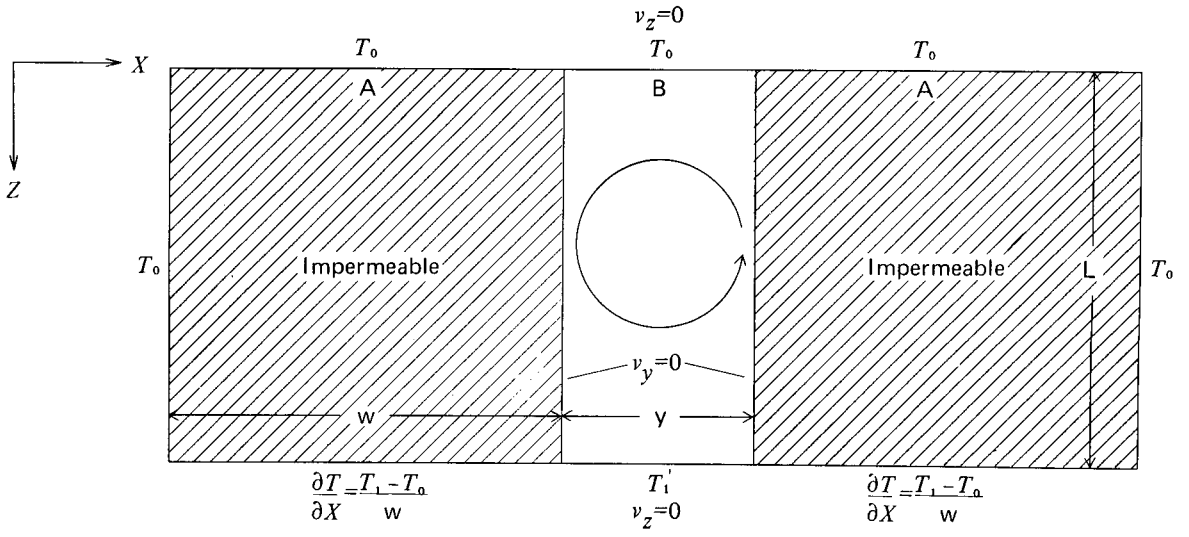

FIGURE 13.—Physical model for cellular convection with conducting side walls.

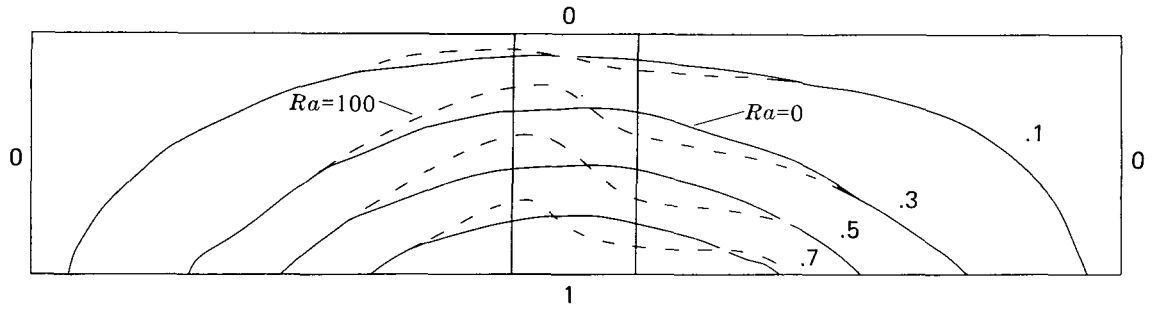

FIGURE 14.—Temperature distributions in convection model with conducting side walls for w/L = 2.1 and y/L = 0.5.

TABLE 3.—*Heat transfer results for convection in vertical channel with conducting side walls*

Location	Q for Ra = 0 (joules/d × 10^7)	Q for Ra = 100 (joules/d × 10^7)	Nu
Top of channel _ _ _	4.38	5.76	1.32
Bottom of channel _	6.41	7.98	1.24
Top of model _ _ _ _	24.4	26.3	−1.08
Bottom of model _ _	29.0	31.0	1.07

A simulation was also performed on the box model in figure 7 with a linear temperature variation imposed along the vertical sides. This simulation also allows heat conduction through the sides and for Ra = 100, Nu = 1.8.

These results indicate that analysis of circulatory convection in bounded reservoirs should provide for the retarding effect of heat conduction through the lateral boundaries. The basic physical model in figure 13 can also be used to simulate the combination of convective throughflow from recharge to discharge areas and circulatory or secondary convection in the upflow channel (Donaldson, 1968, 1970). Results produced by using the program are in agreement with the general features of Donaldson's combined throughflow and secondary convection results; these results indicate that the amount of heat transferred by the secondary flow decreases markedly as the throughflow increases. Numerical analysis of this basic model, including recharge channel(s) at the sides and a reservoir at the base, could utilize more complex boundary conditions and parameter variations to simulate conditions in a specific hydrothermal system.

TWO- AND THREE-LAYER MODELS

For the case of convection in a laterally extensive reservoir, we could remove the restrictive assumption of constant T along the upper and lower surfaces by considering a multi-layer system with less permeable rock above and below the reservoir. Convective flow in the reservoir would not draw heat evenly from below and heat would not be conducted evenly across the top of the layer. Consequently, isotherms in the less permeable layers would be bent near the contacts with the permeable layer in contrast to the constant temperature contacts in the single-layer model.

Donaldson (1962) analyzed the magnitude of this effect for a two-layer system with a permeable layer underlain by an impermeable layer. Both zones had the same finite thickness and were of infinite lateral extent; the upper surface of the permeable layer and the lower surface of the impermeable layer were held at constant temperatures. Donaldson found that the value of Ra_c was lower in the double-layer case than in the single-layer case, but that the conducting layer tended to retard convection effects for values of Ra above the Ra_c.

Several runs using the program were made to compare the results with Donaldson's results and to extend the models to the three-layer case. The multilayer-models are illustrated in figure 15. An equivalent Rayleigh number was computed using the vertical temperature difference across the permeable layer which would exist with heat flow by conduction only and the thickness L of the permeable layer. In table 4, the steady state Nusselt numbers for each model for Ra = 100 are listed. The retardation effect noted by Donaldson is evident in the decrease in Nu from 2.60 for one layer to 1.19 for three layers; although for an aspect ratio of 1.0, the Nusselt number for the three-layer system may have been closer to that for the two-layer case.

TABLE 4.—*Effect of multiple layers on heat transfer in permeable layer with circulatory convection*

[S = cell aspect ratio]

Model	Ra	S	Nu
1 Layer - - - - - - - -	100	1.0	2.60
2 Layers - - - - - - - -	100	1.0	1.34
3 Layers - - - - - - - -	100	.8	1.19

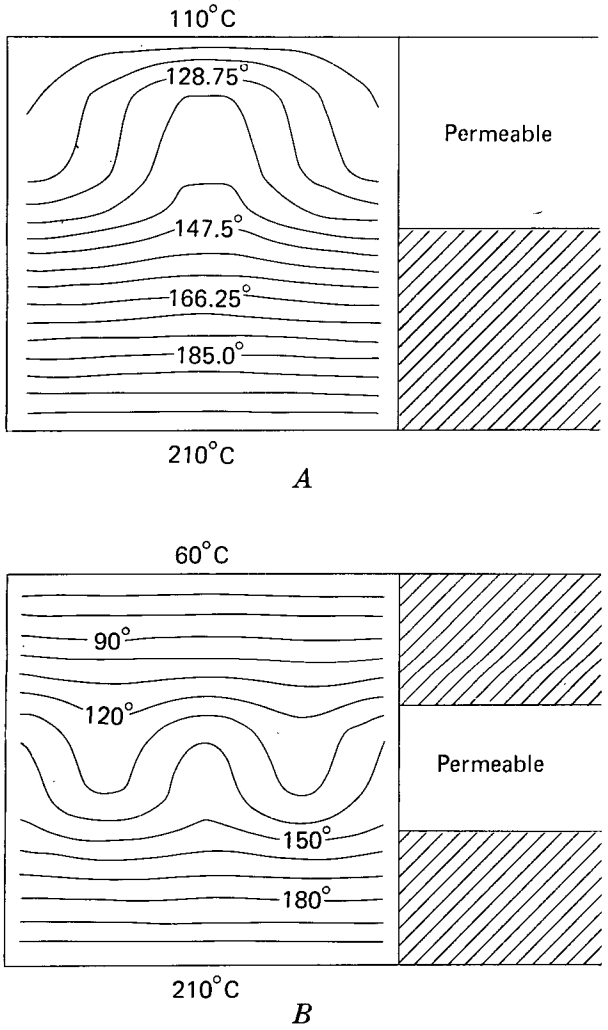

FIGURE 15.—*A*, Isotherms for two-layer model with Ra = 100; *B*, Isotherms for three-layer model with Ta = 100.

The corresponding temperature distributions in the multilayered systems as plotted in figure 15 show the distortion of the isotherms in the impermeable layers near the contacts with the convecting layer. Near the constant temperature boundaries, the isotherms flatten out but are more closely spaced than if there were no convection. This effect raises the question of how deep to place the constant temperature lower boundary to minimize its influence on simulating the convective system. We can use an analysis by Birch (1967) of the temperature distribution beneath the sea floor to show that the isotherm distortion decays as $e^{-\pi z/x'}$, where z = distance from the convective boundary and x' is the distance from peak to trough for a sinusoidal isotherm at $z = 0$. For $\pi z/x' = 2$, the isotherm distortion would be less than 10 percent of the value at $z = 0$. Hence, distortion will be small at the outer boundaries of the multilayer models if $x' < z$, that is if the thickness of the impermeable layer exceeds the peak to trough distance (the width of the convection cell). Since x' must be equal to or less than the thickness of the permeable layer L, $z \geq L$ ensures sufficient thickness for the impermeable layer.

HOT SPRING MODELS

In many of the potential geothermal areas in California and Nevada, the convective and conductive heat flow in and around hot springs are the dominant features in the near-surface thermal regime and account for most of the heat discharge from these areas (Sorey and Lewis, 1975; Olmsted and others, 1975). Commonly, information from deep drilling as to the location and properties of the reservoir or reservoirs supplying the hot spring discharge does not exist. However, we would expect to find fluid and rock with relatively high heat content in and around the hot springs at depths considerably shallower than the underlying reservoirs which may be at depths of 1–5 km (Olmsted and others, 1975). The shallow occurrence of hot fluid and rock suggests the possibility of extraction of energy from relatively shallow depths in these areas of natural discharge, either by capturing the hot spring discharge or the injection and withdrawal of fluid from another source. The feasibility of this approach has been demonstrated at the Casa Diablo Hot Springs in Long Valley, California (McNitt, 1963).

To describe the transfer processes associated with an upflowing hot spring system, the effects of conductive heat losses, mixing, subsurface discharge, and boiling need to be accounted for. Geochemical techniques, including those based on concentrations of silica and the ratio of concentrations of the cations Na, K, and Ca in the hot spring water can provide estimates of the source temperature at depth for the spring water (Fournier and others, 1974). In some cases, the amount of colder, fresher ground water mixing with the thermal water can be determined from the chemistry and enthalpy of the spring discharge. However, to quantify the amount of heat loss by conduction away from the spring conduit and the resultant temperature drop in the spring water, we need to use a numerical model. In addition, it is of interest to analyze the thermal and hydrologic regimes in the rock adjacent to the spring conduit under conditions of circulatory convection and in the absence of convective motions.

For the simplest model, we assume an isolated cylindrical conduit with vertical orientation surrounded by impermeable rock as in figure 16. The lower boundary is formed by the top of a reservoir with fluid at

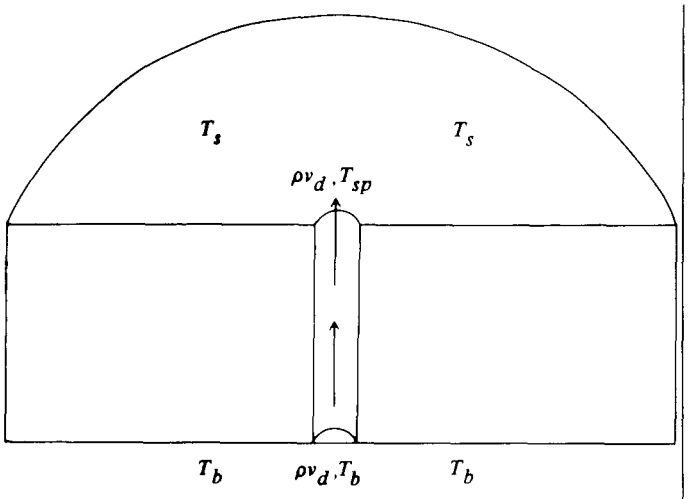

FIGURE 16.—Isolated cylindrical conduit hot spring model.

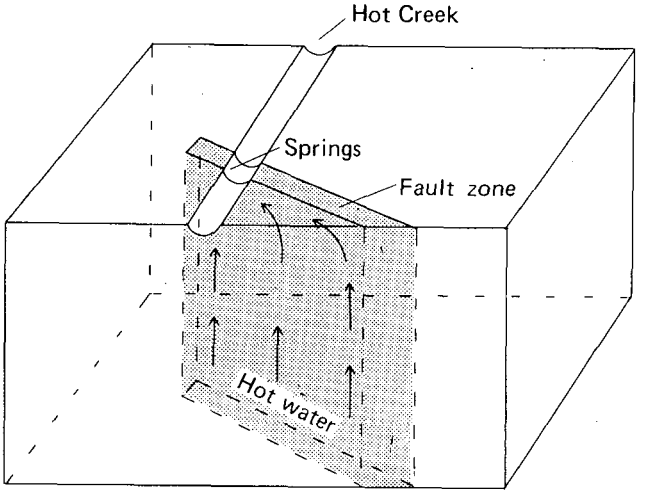

FIGURE 17.—Fault plane hot spring model.

temperature T_b and the upper boundary is the land surface at temperature T_s. The model is extended far enough laterally to justify an insulated boundary condition on the sides. Water enters the bottom of the conduit with temperature T_b at some constant mass flow rate ρv_d. As the fluid moves up the conduit, heat is conducted into the adjacent rock and the fluid temperature falls. The fluid emerges at the land surface at temperature T_{sp} and the conductive heat loss from the conduit is discharged at the land surface within an area of above normal heat flow. Note that the constant temperature T_s is imposed on the land surface up to the edge of the spring conduit but that the temperature of the spring discharge is not fixed. This condition is possible numerically by neglecting heat conduction across the spring surface.

Another possible model for heat transfer in a hot spring system involves water moving up over a more extensive fault plane and then converging near the surface as shown in figure 17. In a specific area, the applicability of the fault plane model over the cylindrical model can be judged from data on the thermal regime adjacent to the springs (Olmsted and others, 1975) and from hydraulic considerations of upward velocities permitted by the available head and conduit permeability (Sorey and Lewis, 1975). It is important to make this distinction, because for the same total spring discharge, the plane model would have considerably greater area for conductive heat loss and lower fluid velocity than the cylindrical model, and therefore greater heat loss and temperature drop.

Mathematical analysis of these models is facilitated by combining the relevant parameters in energy balances for the upflowing fluid columns. Geometries and boundary conditions for each model are illustrated in figure 18. As an approximation, the fault plane model is treated as 2-dimensional and plane symmetric, and the mass flux rate is computed as the total spring discharge divided by the area of upflow. For the cylindrical model, neglecting heat conduction in the vertical direction,

$$2\pi r_c K_m \left.\frac{\partial T}{\partial r}\right|_{r_c} = \rho v_d c \pi r_c^2 \frac{\partial T}{\partial z} \tag{37}$$

which can be rearranged as

$$\frac{\rho v_d c r_c}{2K_m}\frac{\partial T}{\partial z} = \left.\frac{\partial T}{\partial r}\right|_{r_c}. \tag{38}$$

Substituting $\Theta = (T-T_s)/(T_b-T_s)$, $r' = r/r_c$, and $z' = z/L$ we obtain

$$M_c \frac{\partial \Theta}{\partial z'} = \left.\frac{\partial \Theta}{\partial r'}\right|_1 \tag{39}$$

where $M_c = \rho v_d c r_c^2/2K_m L$ = dimensionless mass flow rate in the cylindrical spring conduit. Integration of (39) from $z' = 0$ to $z' = 1$ yields

$$M_c(\Theta_{sp}-1) = \int_0^1 \left.\frac{\partial \Theta}{\partial r'}\right|_1 dz' = Q_c \tag{40}$$

where $\Theta_{sp} = (T_{sp} - T_b)/(T_b - T_s)$ = dimensionless spring temperature at land surface and Q_c = dimensionless radial heat loss from the cylinder. A similar development for the fault plane model in figure 18 yields

$$M_p(\Theta_{sp}-1) = Q_p \tag{41}$$

where $M_p = \rho v_d c W^2/K_m L$ = dimensionless mass flow rate in fault plane conduit and Q_p = dimensionless radial heat loss from plane.

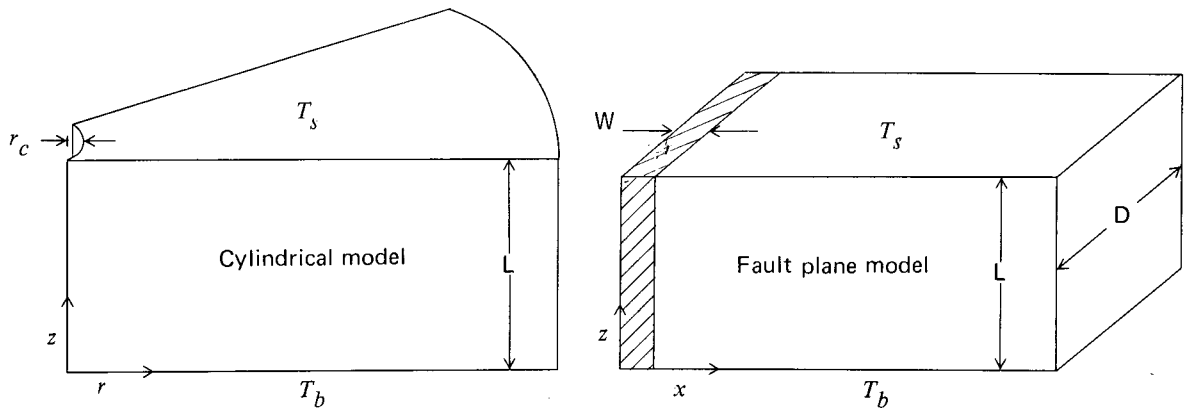

FIGURE 18.—Geometry of hot spring models.

For numerical analysis of heat transfer in these models, a grid of 150 nodes with grid spacing increasing with distance from the spring and depth below land surface was used. The fluid mass flux and temperature were prescribed at the base of the conduit and the same mass flux was removed at the top of the conduit. The initial temperature condition was the conduction-only solution with $\partial T/\partial z = (T_b - T_s)/L$ everywhere, and following the initiation of springflow, transient and steady state solutions were obtained for a range of mass flow rates. Results for cases where the rock surrounding the spring is impermeable are shown in figure 19, in terms of the relationships between M_c, M_p and $(1 - \Theta_{sp})$.

For both models, as the flow rate goes to zero, $(1-\Theta_{sp})=(T_b-T_{sp})/(T_b-T_s)$ approaches 1.0, that is, the spring temperature approaches the land surface temperature. Unfortunately, the relationships expressed by equations 40 and 41 are not unique because Q_c depends on L and r_c and Q_p depends on L and W. The solid curves shown in figure 19 were obtained for the parameters r_c=6 m, W=10 m, and L=1 km. Portions of additional curves for other parameter values as shown by the dashed lines indicate that variations in $(1-\Theta_{sp})$ for a given dimensionless mass flow rate are within about 20 percent of the values computed from the solid curves for parameter values varying by a factor of 2.

For an example of the use of figure 19, consider spring flow in a cylindrical conduit of radius r_c = 6 meters and depth L = 1 km and a fault plane of half-width W = 10 meters, length D = 1 km, and depth L = 1km. For a total mass flow of 1.1×10^5 kg/day, with $T_b - T_s$ = 180°C−10°C, $K_m = 2 \times 10^{-3}$ cal/(sec °C cm), and c = 1 cal/gm°C, the corresponding values of M_c and M_p are 1.00 and 0.031. From figure 19, $(1-\Theta_{sp})$ = 0.11 and 0.61 for the cylinder and plane, respectively. These values correspond to a temperature drop of 18°C and a spring surface temperature of 162°C for the cylindrical model and a temperature drop of 104°C and spring surface temperature of 76°C for the plane model. The total lateral conductive heat loss from spring conduit can be computed for the cylinder as

$$Q = 2\pi K_m L(T_b - T_s)\, Q_c \qquad (42)$$

and for the fault plane as

$$Q = 2K_m L(T_b - T_s)\, (D/W) Q_p \cdot \qquad (43)$$

These equations yield, for the example above, heat losses of 2.3×10^4 cal/sec and 1.3×10^5 cal/sec for the cylinder and plane.

The steady state temperature distribution in the impermeable rock adjacent to the fault plane model considered above is shown in figure 20. The isotherm pattern for the cylindrical model is similar in cross section. Distortion of the isotherms due to the spring flow occurs in a zone within about 1 km of the fault, and the excess heat is conducted upwards toward the land surface. As anticipated, conductive heat losses from the conduit are considerably larger in the upper portion near the land surface than at depth. For this reason, the boundary conditions at the land surface should have a significant influence on spring temperatures near the surface. One complication to consider is that by imposing a constant temperature T_s at the land surface, a singularity in heat flow exists at the wall of the conduit. Numerically, the infinite temperature gradient is avoided by averaging over finite distances; but in actual hot spring areas, the land surface temperature increases considerably near the spring. Thus, a more realistic boundary condition would be the linear heat transfer or radiation boundary condition

$$K_m \frac{\partial T}{\partial z} = H\, T, \text{ at } z = L \qquad (44)$$

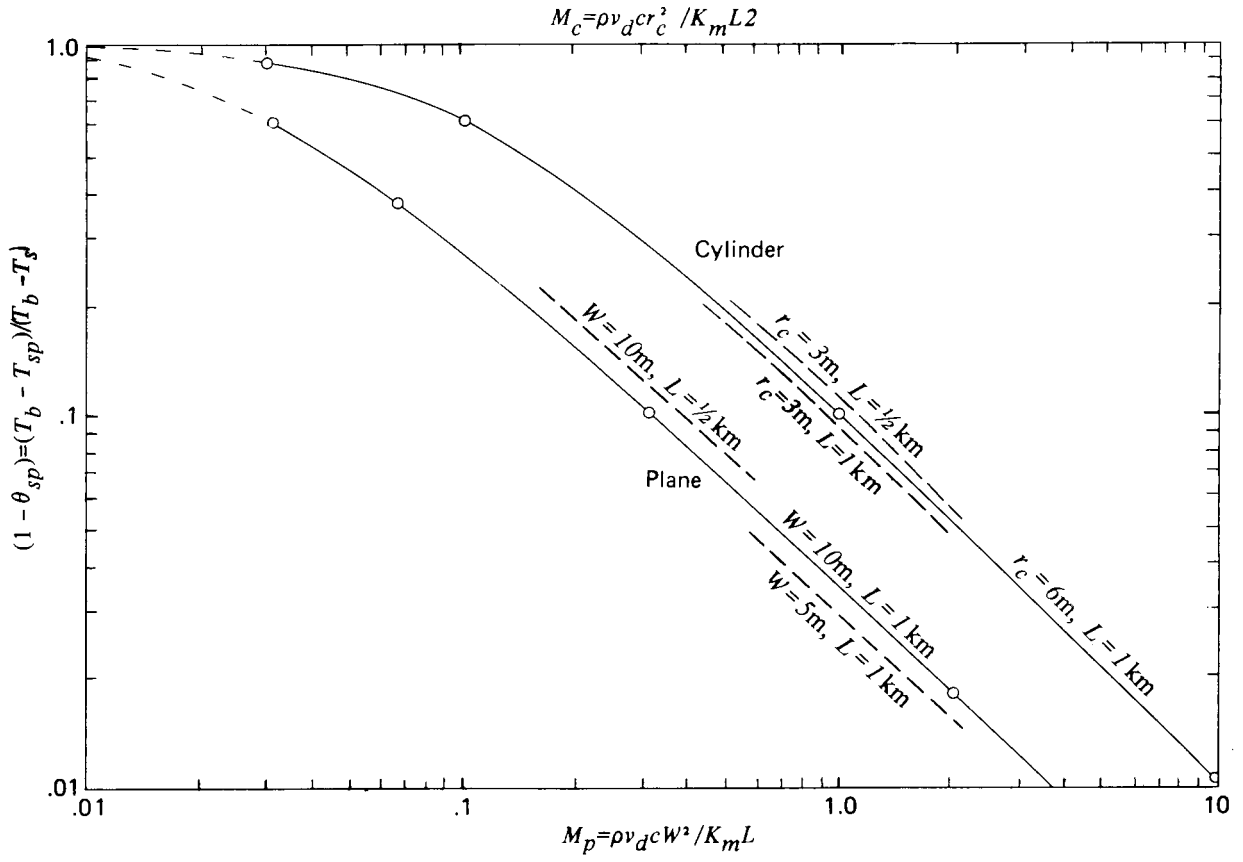

FIGURE 19.—Relationships between dimensionless flow rates (M_c, M_p) and dimensionless temperature drop ($1-\Theta_{sp}$) due to conductive heat loss in cylindrical and fault plane hot spring models.

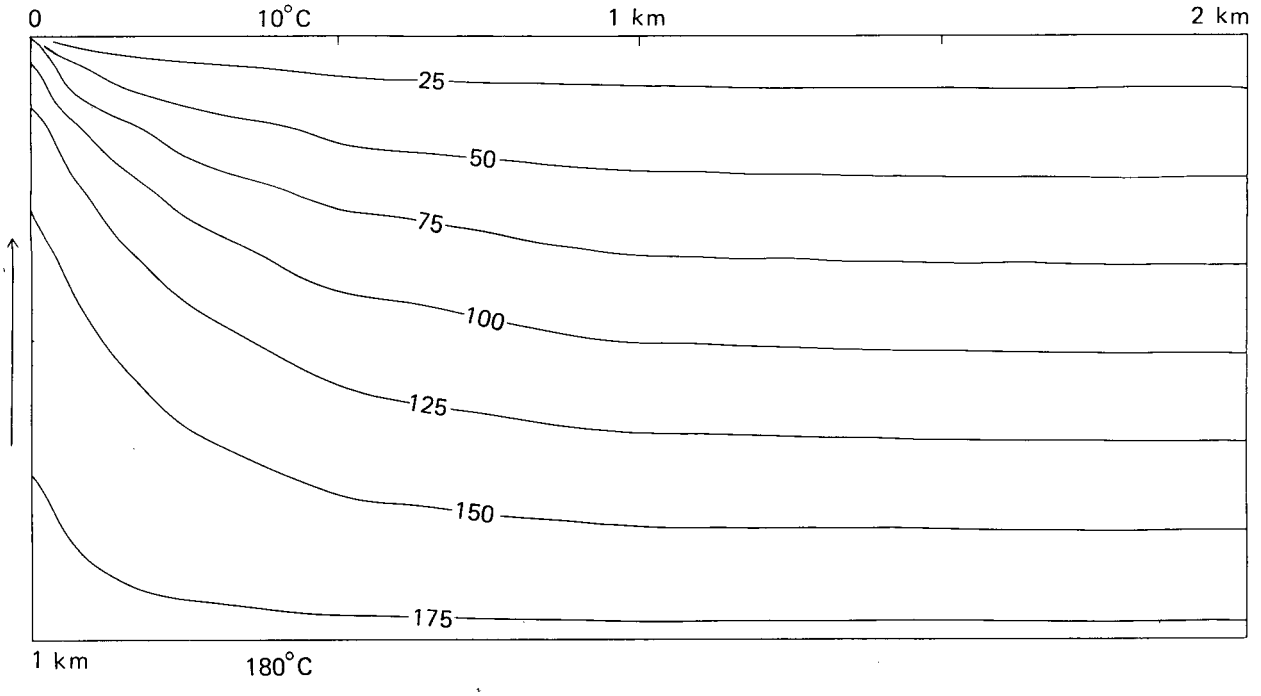

FIGURE 20.—Steady state temperature distribution in fault plane hot spring model with discharge = 10^5 kg/d, W = 10 m, D = 1 Km, and Ra = 0 (k = 0).

where H = coefficient of surface heat transfer (Carslaw and Jaeger, 1959, p. 19). This radiation boundary condition reduces to the constant temperature boundary condition as $H \rightarrow \infty$ and to an insulated boundary condition as $H \rightarrow 0$. An upper limit for H could be obtained from experimental data on turbulent air flow over flat plates. For example, Rohsenow and Choi (1961, p. 200) give

$$H = 1.5 \times 10^{-3}(\rho c v)_{air} \qquad (45)$$

which for air at 15°C yields the following relationship at the land surface between H and mean annual wind velocity v.

v (cm/sec)	H (cal/sec °C cm²)
10	4.5×10^{-6}
100	4.5×10^{-5}
1000	4.5×10^{-4}

Other factors complicate the choice of an effective value of H, such as intermittent air flow, evaporation, and the presence of a dry, low conductivity soil layer. In the latter case, we could relate a particular value of H to a low conductivity layer of thickness $l = K_m/H$. For example, for $K_m = 0.5 \times 10^{-3}$ cal/sec °C cm, l ranges from 0.01 to 1.1 meters for H between 4.5×10^{-4} and 4.5×10^{-6} cal/sec °C cm², respectively. In this study, the effect of using the radiation boundary condition (44) was examined for a range of H from 10^{-6} to 10^{-4} cal/(sec °C cm²).

Results are tabulated in table 5 for the fault plane case considered previously with spring discharge equal to 1.1×10^5 kg/day.

TABLE 5.—*Spring temperature, T_{sp}, total conductive heat loss, Q, and heat flux at land surface near spring, q, for selected values of coefficient of surface heat transfer H*

H (cal/sec °C cm²)	T_{sp} (°C)	Q (cal/sec)	$q(x = 5\text{m})$ (μ cal/sec-cm²)
∞	76.3	1.29×10^5	82
10^{-4}	76.9	1.29×10^5	79
10^{-5}	78.9	1.27×10^5	73
10^{-6}	91.8	1.13×10^5	43

For values of H greater than about 10^{-4}, the radiation boundary condition yields essentially the same results as the constant temperature boundary condition. However, for $H < 10^{-5}$, the spring temperature is significantly greater and the total conductive heat loss and land surface heat flux near the spring less than for the constant temperature case. The temperature distribution for $H = 10^{-6}$ cal/sec °C cm² is shown in figure 21. Land surface temperatures and heat flows vary from 53°C and 43 HFU at a distance of 5 meters to 13.5°C and a normal conductive heat flux of 3.5 HFU beyond about 1 km from the spring. Thus, if the effective values of heat transfer coefficient in field areas are below 10^{-5}, the radiation boundary condition should be used in simulating the near surface thermal

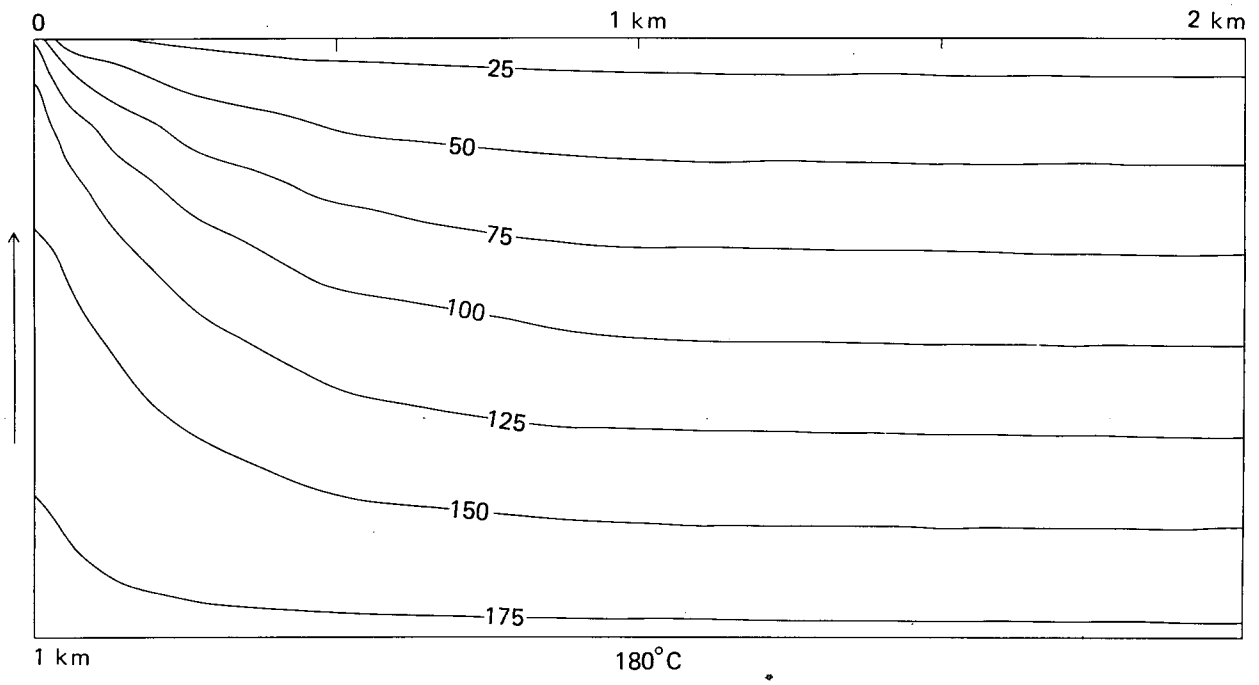

FIGURE 21.—Steady state temperature distribution in fault plane hot-spring model with discharge = 10^5 kg/d, W = 10 m, D = 1 Km, and Ra = 0 (k = 0), and $H = 10^{-6}$ cal/sec°C cm² at land surface.

regime. It should also be noted that we are ignoring the details of heat and mass transfer at the surface in the spring. Many factors such as the geometry of the spring orifice, presence or absence of lateral discharge, and evaporative cooling may cause considerable variations in actual temperatures near the surface.

It is of interest to consider the time required for the conductive thermal regime to reach equilibrium following the development of the spring system. From equation 32, the effective time constant for this 2-dimensional heat transfer problem could be approximated by the expression $L^2 \overline{\rho c}/4K_m$, where L^2 can be thought of as the area through which heat flows from the spring to the land surface. For example, from figure 20, L^2 might represent an area 1 km deep by 1 km wide or 1 km^2. This means that the time constant in this case would be about 9×10^6 days or 25,000 years. The transient numerical simulations for this problem show that temperatures are within 0.1°C of equilibrium after a period of about 50,000 years, or twice the effective time constant. The thermal diffusivity in this problem was a relatively low 0.0032 cm^2/sec; equilibrium times for larger diffusivities would be proportionately smaller.

If the restriction is removed that the rock adjacent to the spring is impermeable, ground-water circulation in this region will affect the thermal regime. Even if the rock permeability is low enough that the critical Rayleigh number of $4\pi^2$ is not exceeded, the fluid would still be unstable because of the high temperature boundary formed by the spring conduit. In modeling this problem numerically, the simplification is made that there is no hydraulic connection between the spring conduit and the adjacent ground-water system. To simplify the problem, a thin impermeable zone is included at the contact between the two regions; such a zone may exist in many field situations where chemical deposition has sealed off the conduit from the surrounding rock.

Once again, consider the fault plane model analyzed previously, that is, discharge = 1.1×10^5 kg/day, $T_b - T_s$ = 180°C − 10°C (fig. 20), but with a rock permeability of 1 millidarcy (10^{-15} m^2). In the absence of spring flow, the equivalent Rayleigh number for this case would be 20. With spring flow, the steady state temperature distribution shown in figure 22 would result. The existence of convection cells is not clearly delineated by the isotherm pattern although comparison with the 125°C and 150°C isotherms from figure 20 show the shifts caused by upflowing fluid near the conduit and downflowing fluid to a distance of about 1.5 km. The actual velocity distribution includes 3 convection cells but with the magnitude of convection decreasing with distance from the spring. As a result of the convection, the temperature drop and total conductive heat loss from the spring are about 6 percent less than for the corresponding impermeable rock case. The 25°C isotherms in figure 22 indicate that

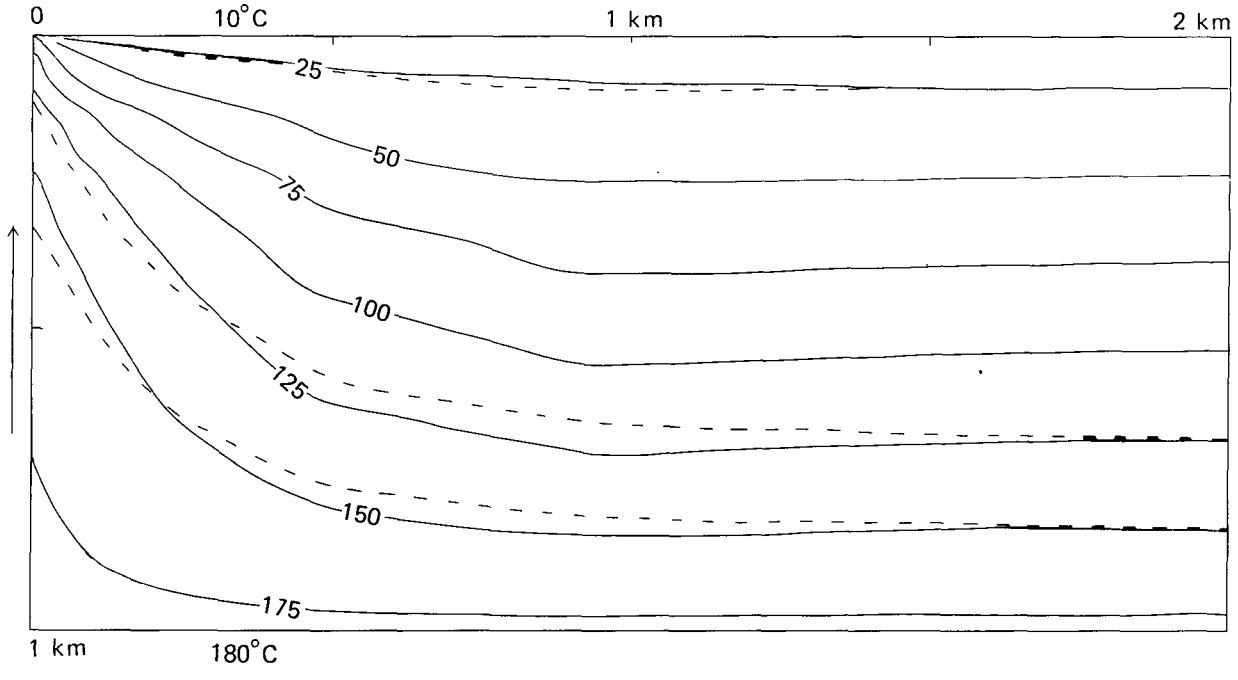

FIGURE 22.—Steady state temperature distribution in fault plane hot-spring model with discharge = 10^5 kg/d, W = 10 m, D = 1 Km, Ra = 20 (solid lines), Ra = 0 (dashed in fig. 20).

heat flow near the land surface is not appreciably affected by convection in the rock below. Similar results in terms of slight lowering of the conductive heat loss from the conduit and negligible changes in heat flow near the land surface were found for other spring discharge rates in systems with Rayleigh numbers below Ra_c although the distortion of the temperature distribution at depth increases somewhat for the higher spring discharge rates.

Now, if the rock permeability is increased to 10 millidarcies (10^{-14} m^2), the Rayleigh number would be 200; and for a discharge of 1.1×10^5 kg/d the resultant temperature distribution is plotted in figure 23. In this case the influence of cellular convection set up by the constant temperature boundaries at the top and bottom of the model dominates the thermal regime. The effect of the hot spring is evident out to a distance of about 0.5 km over which the 100°C and 125°C isotherms show reversals characteristic of cellular convection at large Ra. In this case, convection in the rock causes a more substantial lowering of the conductive heat loss from the spring conduit—0.99×10^5 cal/sec versus 1.29×10^5 for the $Ra = 0$ case—and a temperature drop of 84°C compared with 104°C for $Ra = 0$. The relative effects of the conductive heat loss from the conduit and the enhanced heat transfer caused by convection in the rock are indicated near the land surface by the more closely spaced isotherms between 0 and 0.5 km from the spring compared with the spacing at corresponding intervals beyond 1 km.

These results represent preliminary attempts to simulate heat transfer and fluid flow associated with hot spring systems. To model specific field areas, it may be necessary to include nonvertical orientation of the spring conduit, subsurface discharge and recharge, and boiling near the land surface in the simulation. This work is being planned as sufficient data become available from field studies in California and Nevada. As noted previously, energy development in many of these geothermal areas may focus on localized regions of natural discharge. Thus a useful extension of the numerical modeling work described here will be the evaluation of various schemes for energy development.

SUMMARY AND CONCLUSIONS

We have discussed the development of a numerical code which can treat problems involving slightly compressible fluid and heat transfer in multidimensional porous media. Solutions to the appropriate partial differential equations are obtained by the integrated finite difference method which is essentially equivalent to balancing mass and energy over finite subregions or elements. The resultant system of finite difference equations is solved by an iterative procedure, and solutions to the fluid flow and energy equations are coupled by interlacing in time so that the temperature and velocity fields are interdependent. The useful concepts of fluid and thermal time constants as indi-

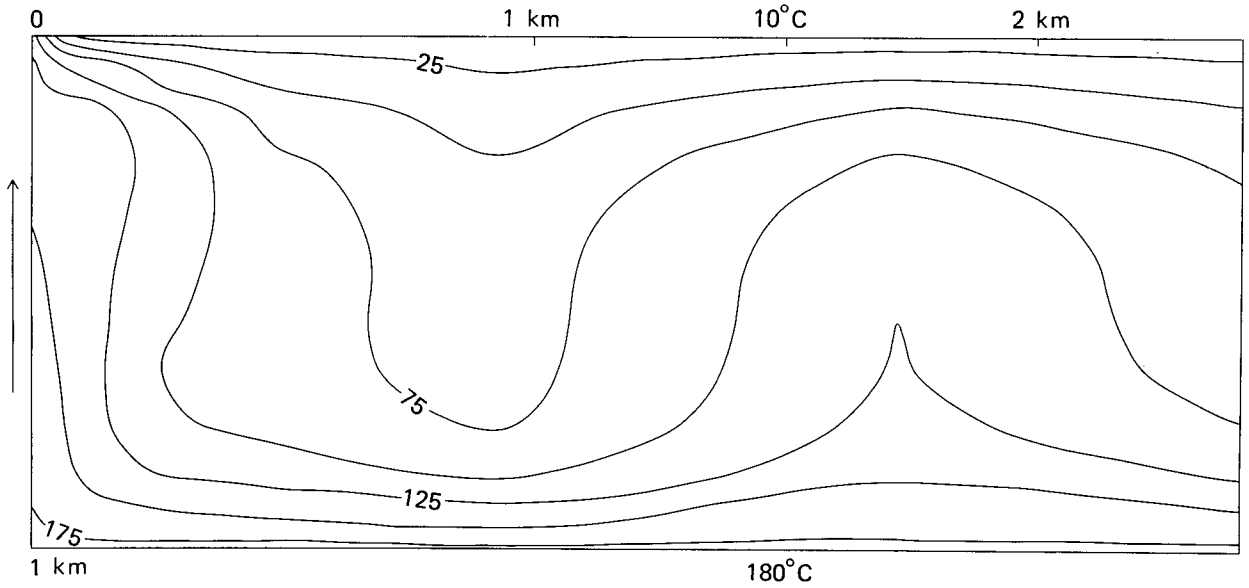

FIGURE 23.—Steady state temperature distribution in fault plane hot-spring model with discharge = 10^5 kg/d, W = 10 m, D = 1 Km, and Ra = 200.

cators of nodal response times and numerical stability limits are an inherent part of the numerical scheme.

In applying the numerical model to the problems of circulatory convection in saturated porous media, the relevant aspects have been discussed as they pertain to geothermal systems, and we find that results from the program on the relationship between the Rayleigh number and the dimensionless heat transfer coefficient or Nusselt number are in good agreement with numerical and experimental results from other authors. Then the numerical model was used to extend these results to include the effects of temperature dependent parameters and density variations with pressure. Variations in fluid viscosity and thermal expansivity with temperature result in substantial differences in the values of the critical Rayleigh number for the onset of convection and the Rayleigh number-Nusselt number relationship compared with corresponding constant parameters results. However, consideration of fluid density as a function of pressure produced no noticeable effect on convective motion.

Numerical simulations of more realistic models for circulatory convection show that for laterally bounded reservoirs, conduction of heat across the vertical side walls results in significant lowering of the rate of vertical heat transfer through the reservoir. For a laterally extensive reservoir, consideration of impermeable or less permeable layers above and below the convecting layer removes the restrictive assumption of constant temperature boundaries on the permeable layer and has the effect of lowering the value of the critical Rayleigh number Ra_c while retarding convective heat transfer at values of Ra above Ra_c.

Heat and mass transfer associated with hot spring systems was analyzed to determine the amount of heat lost by conduction to the rocks surrounding the spring conduit. An isolated cylindrical conduit model and a fault plane conduit model were considered, and the temperature drop in the hot spring water between the source reservoir and the surface due to conductive heat loss was determined numerically as a function of flow rate. The steady state temperature distribution for the case where the rock surrounding the spring is impermeable shows that heat loss from the spring distorts the normally horizontal position of the isotherms out to distances comparable to the depth of the spring conduit. Conductive heat flux at the land surface is high near the spring but near the normal or background level beyond one conduit depth. The time required for the conductive thermal regime to equilibrate following the development of hot spring activity can be approximated by the expression $L^2\overline{\rho c}/2K_m$ where L is the depth to the source reservoir. For unconsolidated sediments with low thermal conductivity, the equilibration time is about 50,000 years for a reservoir at 1 km.

The effects of fluid circulation in the rock surrounding the spring conduit were examined for systems in which the equivalent Rayleigh number (in the absence of hot spring activity) was both above and below the critical value of $4\pi^2$. With $Ra<4\pi^2$, circulatory convection is set up due to the presence of the hot spring, but it causes only slight effects on the thermal regime in the rock surrounding the spring conduit and on the conductive heat loss and temperature drop associated with the spring. For the case with $Ra>4\pi^2$, circulatory convection resulting from the temperature difference T_b-T_s between the source reservoir and the land surface dominates the thermal and hydrologic regimes and significantly reduces the conductive heat loss and temperature drop for the spring.

The results of this investigation demonstrate the usefulness of numerical modeling to describe the natural conditions of heat transfer and fluid flow in geothermal areas. Given preliminary thermal, hydrologic, geophysical, and geochemical information, it is possible to construct and analyze simplified conceptual models of specific hydrothermal systems as a guide to further data collection in undeveloped areas. An application of this technique applied to the Long Valley caldera in California is described by Sorey, Lewis, and Olmsted (1978). As sufficient parametric and geometric data become available from deep test drilling to refine the model, it can then be used to evaluate rates and magnitudes of energy recovery and effects of development on existing water resources.

REFERENCES

Bear, J., 1972, Dynamics of fluids in porous media: New York, American Elsevier Pub., 764 p.

Beck, J. L., 1972, Convection in a box of porous material saturated with fluid: Physics of Fluids, v. 15, no. 8, p. 1377–1383.

Birch, F., 1967, Low values of oceanic heat flow: Jour. Geophys. Research, v. 72, no. 8, p. 2261–2262.

Bird, R. B., Stewart, W. E., and Lightfoot, E. N., 1960, Transport Phenomenon: New York, Wiley, 780 p.

Bodvarsson, G., 1961, Physical characteristics of natural heat resources in Iceland: U.N. Conf. New Sources Energy, Rome, 1961, Proc., v. 2, p. 82–89.

Caltagirone, J. P., Cloupean, M., and Combarnous, M. A., 1971, Fluctuating natural convection in a horizontal porous layer [in French]: Acad. Sci., [Paris], Comptes rendus, B, v. 273, no. 20, p. 833–836.

Carslaw, H. S., and Jaeger, J. C., 1959, Conduction of heat in solids: London, Oxford Press, 510 p.

Coats, K. H., George, W. D., Chu, C., and Marcum, B. E., 1973, Three-dimensional simulation of steam flooding: Soc. Petrol. Engr. Jour., v. 15, no. 6, p. 573–592.

Combarnous, M. A., and Bories, S. A., 1973, Thermal convection in saturated porous media: Groupe D'etude Sur Les Milieux Poreux, Institut Francais Du Petrole, Toulouse, Rapport G. E. 11.

Curry, D. M., 1970, Multi-dimensional analysis of heat and mass transfer in porous media: Houston, Texas, University of Houston, unpublished Ph. D. thesis, 197 p.

Darcy, H. P. G., 1856, Les Fontaines Publignes de la Villa de Dijon: Paris, Victor Dalmont, 647 p.

Donaldson, I. G., 1962, Temperature gradients in the upper layers of the earth's crust due to convective water flows: Jour. Geophys. Res., v. 67, no. 9, p. 3449–3459.

_____ 1968, A possible model for hydrothermal systems and methods of studying such a model: Third Australian Conf. on Hydraulics and Fluid Mechanics, Nov. 25–29. Paper 2580.

_____ 1970, The simulation of geothermal systems with a simple convective model: Geothermics, Spec. Issue 2, U.N. Symposium on the Development and Utilization of Geothermal Resources, Pisa, Italy, v. 2, pt. 1, p. 649–654.

Dorsey, N. E., 1968, Properties of ordinary water-substance: New York, Hafner Pub. Co., 673 p.

Edwards, A. L., 1969, TRUMP: A computer program for transient and steady-state temperature distributions in multidimensional systems: Natl. Tech. Inf. Service, Springfield, Virginia, UCRL 14754, Rev. 2, 22151, 263 p.

Einarsson, T., 1942, The nature of springs of Iceland (in German): Rit. Visind. Es., 26, 91 p.

Elder, J. W., 1957, Some problems in fluid dynamics: Cambridge, England, Cambridge University, unpublished Ph. D. thesis.

_____ 1966, Heat and mass transfer in the earth: Hydrothermal Systems, New Zealand, D.S.I.R. Bull. 169, 115 p.

Faust, C. R. and Mercer, J. W., 1975, Mathematical modeling of geothermal systems [abs.]: Proc. of Second U.N. Symposium on Development and Use of Geothermal Resources, San Francisco, Calif., May 20–29, 1975, v. 3, p. 1635–1641.

Fernandez, R. T., 1972, Natural convection from cylinders buried in porous media: Berkeley, California, University of California, unpublished Ph. D. thesis, 300 p.

Fournier, R. O., White, D. E., and Truesdell, A. H., 1974, Geochemical Indicators of subsurface temperature—Pt. 1, Basic assumptions: Jour. Research U.S. Geol. Survey, v. 2, no. 3, p. 259–262.

Green, D. W., 1963, Heat transfer with fluid flowing through porous media: Oklahoma, University of Oklahoma, unpublished Ph. D. thesis.

Henry, H. R. and Hilleke, J. B., 1972, Exploration of multiphase fluid flow in a saline aquifer system affected by geothermal heating: University of Alabama Bureau of Engr. Research Rept. No. 150–118, 123 p.

Holst, P. H., 1970, A theoretical and experimental investigation of natural convection in porous media: University Calgary, Alberta, Canada, Ph. D. thesis.

Holst, P. H., and Aziz, K., 1972a, A theoretical and experimental study of natural convection in a confined porous medium: Canadian Jour. Chem. Eng., v. 50, p 232–241.

_____ 1972b, Transient three-dimensional natural convection in confined porous media: Int. Jour. Heat and Mass Transfer, v. 15, p. 73–90.

Horne, R. N. and O'Sullivan, M. J., 1974, Oscillatory convection in a porous medium heated from below: Jour. Fluid Mech., v. 66, pt. 2, p. 339–352.

James, R., 1968, Wairakei and Larderello; geothermal power systems compared: New Zealand Jour. Sci. and Technology, v. 11, p. 706–719.

Landau, L. D., and Lifshitz, E. M., 1959, Fluid Mechanics: London, Pergamon Press, 536 p.

Lantz, R. B., 1971, Quantitative evaluation of numerical diffusion (truncation error): Soc. Petroleum Engineers Trans., v. 251, p. 315–320.

Lapwood, E. R., 1948, Convection of a fluid in a porous media: Proc. Cambridge Phil. Soc., v. 44, p. 508–521.

Lasseter, T. J., 1974, Underground storage of liquified natural gas in cavities created by nuclear explosives: Berkeley, California, University of California, unpublished Ph. D. thesis, 273 p.

Lasseter, T. J., Witherspoon, P. A., and Lippman, M. J., 1975, Multiphase multidimensional simulation of geothermal reservoirs: Proc. of Second U.N. Symposium on Development and Use of Geothermal Resources, San Francisco, California, May 20–29, 1975, v. 3, p. 1715–1723.

McNitt, J. R., 1963, Exploration and development of geothermal power in California: California Div. Mines and Geology, Spec. Rept. 75.

Mercer, J. W., 1973, Finite element approach to the modeling of hydrothermal systems: Urbana-Champaign, Illinois, University of Illinois, unpublished Ph. D. thesis, 115 p.

Mercer, J. W., Faust, C., and Pinder, G. F., 1974, Geothermal reservoir simulation: Proc. of National Science Foundation Conference on Research for the development of Geothermal Energy Resources, Pasadena, California, Sept. 23–25, 1974, p. 256–267.

Narasimhan, T. N., 1975, A unified numerical model for saturated-unsaturated groundwater flow: Berkeley, California, University of California, unpublished Ph. D. thesis, 244 p.

Olmsted, F. H., Glancy, P. A., Harrill, J. R., Rush, F. E., and Van Denburgh, A. S., 1975, Preliminary hydrologic appraisal of selected hydrothermal systems in northern and central Nevada: U.S. Geol. Survey Open-File Rept. 75–56, 267 p.

Platzman, G. W., 1965, The spectral dynamics of laminer convection: Jour. Fluid Mech., v. 23, p. 481–510.

Raats, P. A. C., and Klute, A., 1968, Development of equations describing transport of mass momentum and energy in soils, *in* Water in the unsaturated zone, Proc. Wageningen Symposium: Pub. No. 83, International Association of Scientific Hydrology, p. 535–546.

Remson, I., Hornberger, G. M., and Molz, F. J., 1971, Numerical methods in subsurface hydrology: New York, Wiley-Interscience, 389 p.

Rohsenow, W. N., and Choi, H. Y., 1961, Heat, mass and momentum transfer: Englewood Cliffs, New Jersey, Prentice-Hall.

Sorey, M. L., and Lewis, R. E., 1975, Convective heat flow from hot springs in the Long Valley caldera, Mono County, California: Jour. Geophys. Research, v. 81, no. 5, p. 785–791.

Sorey, M. L., Lewis, R. E., and Olmsted, F. H., 1978, The Hydrothermal System of Long Valley caldera, California: U.S. Geol. Survey Prof. Paper 1044–A, 60 p.

Spillette, A. G., and Nielson, R. L., 1968, Two-dimensional method for predicting hot waterflood recovery behavior: Jour. Petroleum Technology, v. 20, p. 627–638.

Sutton, F. M., 1969, Stability of flow in a model of a hydrothermal system: Victoria University, Wellington, New Zealand, unpublished M. Sc. thesis.

Weinstein, H. G., Wheeler, J. A., and Woods, E. G., 1974, Numeri-

cal model for steam stimulation *in* Improved oil recovery symposium, Apr. 22-24, 1974: Tulsa, Oklahoma, Soc. Petroleum Eng. preprint 4759, p. 253–270.

White, D. E., 1957, Thermal waters of volcanic origin: Geol. Soc. America Bull, v. 68, p. 1637–1658.

_____ 1961, Preliminary evaluation of geothermal areas by geochemistry, geology, and shallow drilling, U.N. Conf. New Sources Energy, Rome, Italy, 1961, Proc. v. 2, p. 402–408.

White, D. E., Muffler, L. J. P., and Truesdell, A. H., 1971, Vapor-dominated hydrothermal systems compared with hot-water systems: Econ. Geology, v. 66, no. 1, p. 75–97.

Witherspoon, P. A., Newman, S. P., Sorey, M. L., and Lippman, M. J., 1975, Modeling geothermal systems: Univ. California, Lawrence Berkeley Lab. Rept. 3263, 68 p.

Wooding, R. A., 1957, Steady state free thermal convection of liquid in a saturated permeable medium: Jour. Fluid Mech., v. 2, p. 274.

_____ 1963, Convection in a saturated porous medium at large Rayleigh number or Peclet number: Jour.Fluid Mech., v. 15, p. 527.